University of Heidelberg
Faculty for Chemistry and Earth Sciences

MASTER THESIS
Master´s degree program in Chemistry

SILICA NANOCAPSULES FOR ENZYME REACTIONS

Sarah Lembke
Matriculation number: 3599476

Supervisor: Dr. Sharafudheen Pottanam Chali
Examiners: Jun.-Prof. Dr. Eva Blasco
Prof. Dr. Katharina Landfester

Conducted at the
Max Planck Institute for Polymer Research in Mainz
at the Physical Chemistry of Polymers department
of Prof. Dr. Katharina Landfester

Submitted on the 25th of April 2022

Acknowledgments

Firstly, I want to express my gratitude towards Prof. Dr. Katharina Landfester for the permission to complete this thesis in her research group. The guidance and advice that she provided me have been a great help over the past six months. Furthermore, I want to thank Prof. Dr. Shuai Jiang from the Ocean University of China for taking the time to meet with me and sharing his expertise in the synthesis of silica nanocapsules with me. I greatly appreciate their feedback and the opportunity to learn from their longstanding expertise in this field of research.

I am thankful to Dr. Sharafudheen Pottanam Chali for supervising my work and helping me improve my synthesis strategy. He always took time to discuss my progress and I have greatly benefited from his useful advice and our discussions. I truly appreciate the effort he took in proofreading my thesis. Moreover, I want to thank Laura Dietz for conducting the cell experiments, Christine Rosenauer for conducting the multi-angle DLS-measurements and Christoph Sieber for making the TEM micrographs.

I would also like to thank all members of the Department of “Physical Chemistry of Polymers” at the Max Planck Institute for Polymer Research for introducing me to the equipment and the measurement techniques, as well as for helping me to find my way at the institute in general. The productive environment in the department and admirable cooperation were deeply enriching and helped me to stay motivated during challenging times.

Lastly, I want to express my gratitude towards Jun. Prof. Dr. Eva Blasco for consenting to be the examiner of my master thesis. Without her willingness to take this responsibility, conducting my master thesis in the Department of Prof. Dr. Landfester would not have been possible.

Declaration

I hereby declare that this thesis is the result of my own work carried out in the research group for Physical Chemistry of Polymers of Prof. Dr. Katharina Landfester at the Max Planck Institute for Polymer Research in Mainz between October 2021 and April 2022. All sources of information I have used have been fully identified. Specific references were made in the corresponding passages of the text. I further state that neither this thesis nor any substantial part of it has already been submitted or is being concurrently submitted for a degree or diploma or any further qualification at the University of Heidelberg or any other University or similar institution.

Ich erkläre hiermit, dass diese Arbeit als Resultat meiner eigenständigen Arbeit in der Forschungsgruppe für Physikalische Chemie der Polymere von Frau Prof. Dr. Katharina Landfester am Max-Planck-Institut für Polymerforschung in Mainz im Zeitraum zwischen Oktober 2021 und April 2022 entstanden ist. Jegliche Informationsquellen wurden vollständig identifiziert und die entnommenen Inhalte in den entsprechenden Textpassagen unter Angabe der Quelle kenntlich gemacht. Weder diese Masterarbeit noch erhebliche Teile daraus wurden zuvor oder werden zurzeit zur Erlangung eines akademischen Grades oder einer anderen Qualifikation an der Universität Heidelberg oder einer vergleichbaren Institution eingereicht.

Heidelberg,

Table of contents

1. Abstract

Artificial biological reaction systems rely on the development of efficient enzymatic nanoreactors that can modulate competitive cascade reactions and control their kinetics via co-compartmentalization of multiple enzymes. However, identifying the optimal design poses a major challenge for compartmentalized enzymatic cascade reactions, as the nanoreactors´ efficiency depends on multiple parameters as for example the enzyme concentration, the ratio of the different enzymes, and the transport of substrate and product across the compartment barrier.

In this work, a synthesis strategy for enzyme-loaded silica nanocapsules (SiNCs) in small volumes was developed in order to enable the comparison of various concentrations of encapsulated enzyme for identifying the ideal enzyme concentration for maximum catalytic efficiency. In the employed synthesis, the SiNCs were prepared in an inverse (water-in-oil) miniemulsion. The enzymes were dissolved in the aqueous phase to enable a direct encapsulation during the shell formation and the obtained SiNCs were subsequently transferred to the aqueous medium. During the optimization, high-pressure homogenization was established as the preferable emulsification technique. Moreover, a mixture of tetramethyl orthosilicate (TMOS) and (3-aminopropyl)triethoxysilane (APTES) was proven to yield continuous shells and a dependence of the shell thickness on the amount of used precursors was observed. Moreover, a novel technique employing automatic shaking was introduced for the transfer of nanocapsules to aqueous medium. Lastly, the optimized conditions were employed to synthesize SiNCs containing various concentrations of either glucose oxidase (GOx) or horseradish peroxidase (HRP) and it was observed that the SiNCs exhibit a rapid uptake by HCT 116 cells.

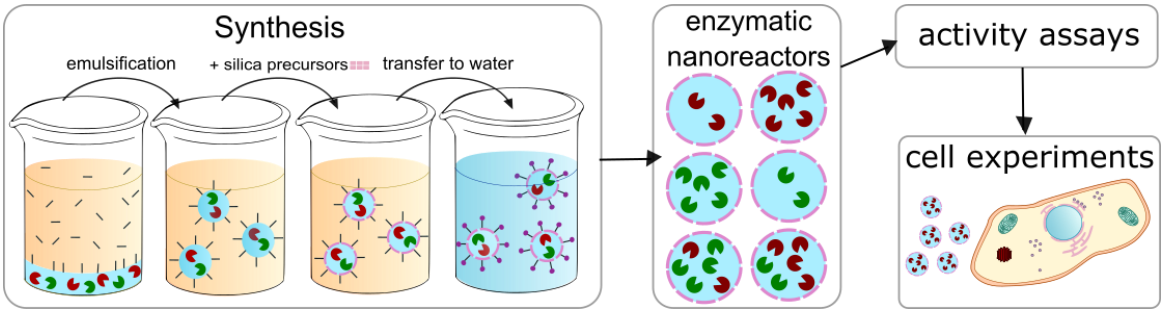

Figure 1: Schematic procedure for optimizing the cascade reaction kinetics for different enzyme concentrations in enzymatic nanoreactors as possible artificial cell organelles.

2. Motivation

The compartmentalization of enzymes into organelles inside eukaryotic cells enables the execution of reactions and metabolic processes with remarkable efficiency. Mimicking these organelles by developing enzyme modules in which several enzymes can be co-compartmentalized is of uppermost importance to create artificial systems for enzymatic cascade reactions.[1]

Silica nanocapsules (SiNCs) are exemplary contenders for such enzyme-containing nanoreactors, because of their well-defined composition and their mesoporous shell enabling the substrate to diffuse inside the capsules and reach the enzymes active site.[2] Moreover, the silica shell provides additional protection from external factors and helps the encapsulated enzymes to retain their activity.[3] In addition to this, siloxane chemistry enables an easy functionalization of the capsule surface with various different moieties, such as targeting ligands and contrast agents.[4] Despite these advantages, SiNCs have only been employed as nanoreactors quite recently, due to the challenges faced when employing an interfacial sol-gel reaction in a miniemulsion process to form a dense silica shell. Recently, Jiang et al.[5] developed a synthesis of semipermeable SiNCs for the quantitative encapsulation of enzymes in an inverse (water-in-oil) miniemulsion. They encapsulated glucose oxidase and horseradish peroxidase to mimic an intracellular catalytic cascade reaction and proved that co-compartmentalization of certain enzymes can be used to regulate the overall kinetics of the cascade reaction.[5]

Studies on how the overall amount of enzyme and the ratio of glucose oxidase to horseradish peroxidase influences the reaction kinetics are still pending in order to optimize the catalytic efficiency of the nanoreactors. Therefore, the development of an optimized synthesis for enzyme-loaded SiNCs in small quantities is an unavoidable necessity to enable the comparison of various enzyme concentrations and ratios. Hence, it was the goal of this work to establish said synthesis to pave the way for studying the kinetics of the cascade reaction in confinement and to enable an optimization of the enzyme concentrations for an application as artificial organelles in living cells.

3. Introduction

3.1 Nanomaterials

The International Union of Pure and Applied Chemistry (IUPAC) has defined nanoparticles as particles that can exhibit any shape but must have at least one dimension in the range of 1 – 100 nm.[6] Correspondingly, the EU commission defined nanomaterials as materials that are manufactured or of natural origin but must possess external dimensions in the 1 – 100 nm size range. Nonetheless, the EU commission acknowledged that there is no scientific evidence to justify a strict upper limit of 100 nm,[7] and other definitions frequently include particles in a range of up to 1000 nm in their conception of nanoparticles.[8] Over the past decades, such well-defined structures with a size of less than a micrometer have allured tremendous research efforts, because of their size-dependent chemical and physical properties and diverse fields of application. Due to their nano size, quantum effects can become predominating and the increased surface to volume ratio in nanoparticles causes their properties to be prevalently dominated by the surface atoms rather than the interior atoms.[9] These properties of nanoparticles that differ from the properties of the bulk material lay the foundation for the great interest in nanoparticles in profuse areas of fundamental research for example biomedicine[10], catalysis[11], or power generation.[12]

The different types of nanoparticles that are depicted in **Figure 2** are commonly sorted into subcategories based on the materials that they are made of. Gold, metal oxide, and silica nanoparticles are examples of nanoparticles that are categorized as inorganic nanoparticles while carbon nanotubes, fullerenes, and graphene are often considered to belong to a separate category of carbon-based nanomaterials. Micelles, liposomes, dendrimers, and polymeric nanoparticles/nanocapsules on the other hand belong to the category of organic nanoparticles.[13]

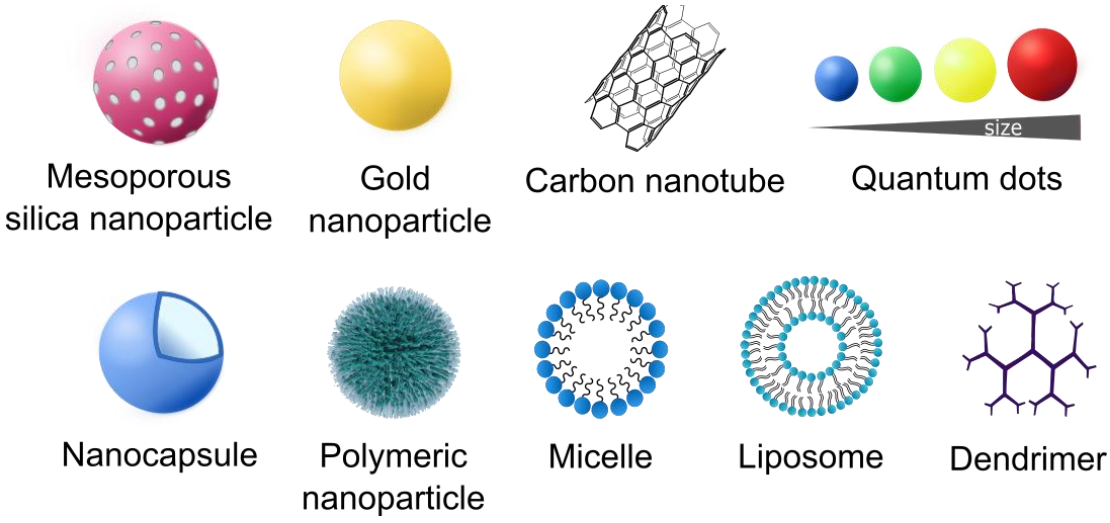

Figure 2: Scheme of different types of nanoparticles, especially for biomedical applications.[14]

In general, nanocapsules are defined as hollow nanoparticles with a solid shell surrounding a cavity in which substances can be entrapped. Therefore, nanocapsules are a morphological subcategory of nanoparticles and can be categorized as either organic or inorganic depending on the material that their shell is made of.[6]

For this versatile pool of different materials, a broad variety of synthesis methods is accessible which are categorized as either top-down or bottom-up approaches. Top-down techniques are methods such as mechanical milling or laser ablation which transform a bulk material into nano-sized particles. While these methods are often simple to use and cost-effective, they are insufficient for synthesizing extraordinarily small particles or particles with complex morphologies and shapes. The bottom-up approach on the other hand is the polar opposite as the nanoparticles are formed by the assembly of molecules or atoms into larger structures. In general, bottom-up techniques yield nanomaterials with well-defined shape, size, and chemical composition making bottom-up techniques the superior method for synthesizing complex nanoparticles.[15] Among the bottom-up techniques, the use of emulsions and droplets is a commonly applied, facile method for fabricating nanoparticles and nanocapsules and the miniemulsion technique employed for this thesis will be discussed in more detail in the following section.

3.2 Miniemulsion technique

An emulsion is a fluid colloidal system consisting of at least two immiscible liquids. Since one liquid is dispersed in the other as liquid droplets or liquid crystals, it is known as the dispersed phase, while the other is known as the continuous phase.[16] A miniemulsion is a special type of such a heterophase system in which the formed nanodroplets are in the size range of 30 to 500 nm. The efficient stabilization of the droplets is obtained by using a surfactant in combination with an osmotic pressure agent. Utilizing such miniemulsions, polymeric and inorganic nanoparticles as well as nanocapsules encapsulating a broad variety of compounds can be synthesized.[17]

When referring to miniemulsions, a distinction is made between direct and inverse miniemulsions. If nonpolar droplets are dispersed in a polar continuous phase (commonly oil-in-water) the miniemulsion is referred to as direct, while an inverse miniemulsion comprises polar droplets and a nonpolar continuous phase (water-in-oil).[18] Since direct miniemulsions were not applied in this thesis, inverse miniemulsions will be discussed to a greater extent. **Figure 3** depicts the process of fabricating an inverse miniemulsion.

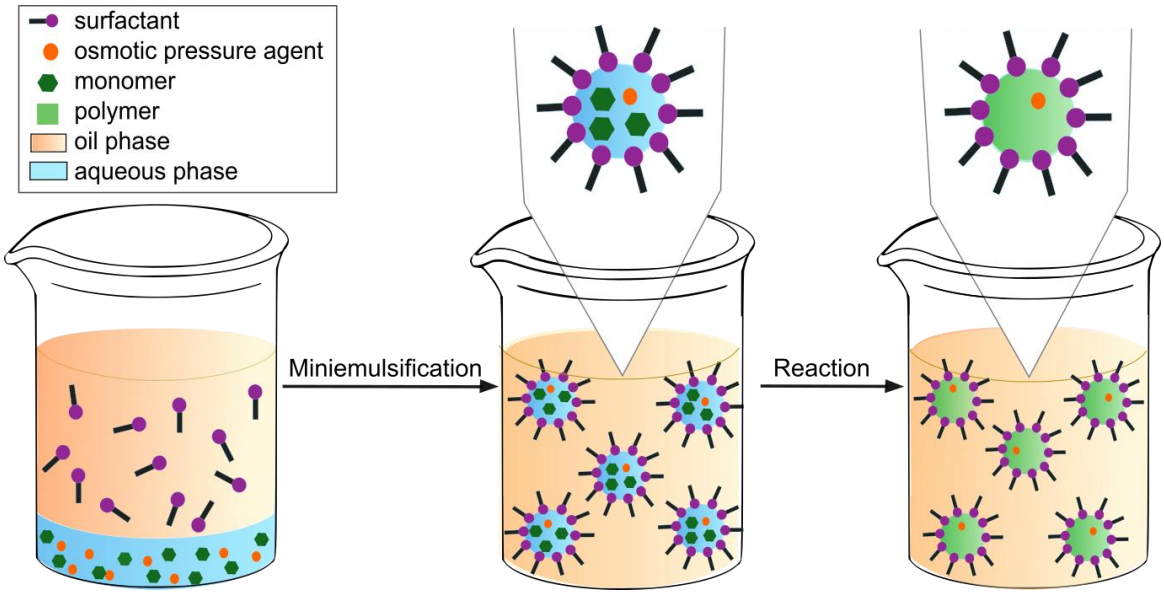

Figure 3: Scheme of the miniemulsion process and nanoparticle formation in an inverse miniemulsion.

Homogenization of a two-phase mixture is usually started by stirring the sample in order to obtain droplets of approximately ten times the size of the final droplets. Afterwards, the miniemulsion is formed by applying high shear forces by for example ultrasonication or high-pressure homogenization. The obtained small droplets exhibit a narrow size distribution and act as independent nanoreactors and the reaction forming the final nanoparticles or nanocapsules can either take place inside or at the interface of these droplets.[19]

In order to preserve the fabricated miniemulsion, the nanoscopic droplets require stabilization against collisions with subsequent coalescence and Ostwald ripening. The former can be averted by employing appropriate surfactants that provide either steric or electrostatic stabilization of the droplets while the latter can be counteracted by the addition of an osmotic pressure agent.[20] Moreover, the surfactant has to be adapted in order to be suitable for either a direct or an inverse emulsion. One criterion for choosing a suitable surfactant is the hydrophilic-lipophilic balance (HLB), a measure to which degree a surfactant is hydrophilic or lipophilic. It ranges from 0 – 20 with high values being equivalent to mainly hydrophilic/lipophobic surfactants and low values for mainly lipophilic/hydrophobic surfactants,[21] which are suitable for the fabrication of inverse miniemulsions.[17]

Since the fabrication of a miniemulsion always leads to minor size differences between the generated droplets, the radius dependent Laplace pressure varies from one droplet to another as shown by the following relation:

$$p_{\mathrm{Laplace}} = \frac{2\gamma}{r}$$

It is apparent that the Laplace pressure inside the droplets depends on the surface tension γ while being inversely proportional to the droplet radius *r,* i.e. the pressure increases with decreasing droplet size.[22] In order to minimize the droplets´ Laplace pressure, a mass flux from smaller to larger droplets occurs. This process called Ostwald ripening leads to the shrinkage and disappearance of smaller droplets while simultaneously swelling larger droplets (**Figure 4**, **A**). The polydispersity, size, and solubility of the dispersed droplets in the continuous phase have an impact on the rate of Ostwald ripening, but it can be counteracted by the addition of osmotic pressure agents also known as co-stabilizers. In a direct miniemulsion these co-stabilizers are hydrophobic compounds such as hexadecane while inverse miniemulsions require the use of lipophobes, for example salts as co-stabilizers.[17]

As shown in **Figure 4**, the osmotic agent is trapped inside the droplets and cannot diffuse from one droplet to another, because it is preferentially located in the dispersed phase and insoluble in the continuous phase. Thereby the osmotic pressure agent counteracts the Laplace pressure by building up an osmotic pressure inside the droplets, which is given by the following equation, where R is the ideal gas constant, *T* is temperature, *M* is molecular weight and *c* is the molar concentration.[19]

$$\Pi_{\mathrm{osm}} = \frac{\mathrm{R}Tc}{M}$$

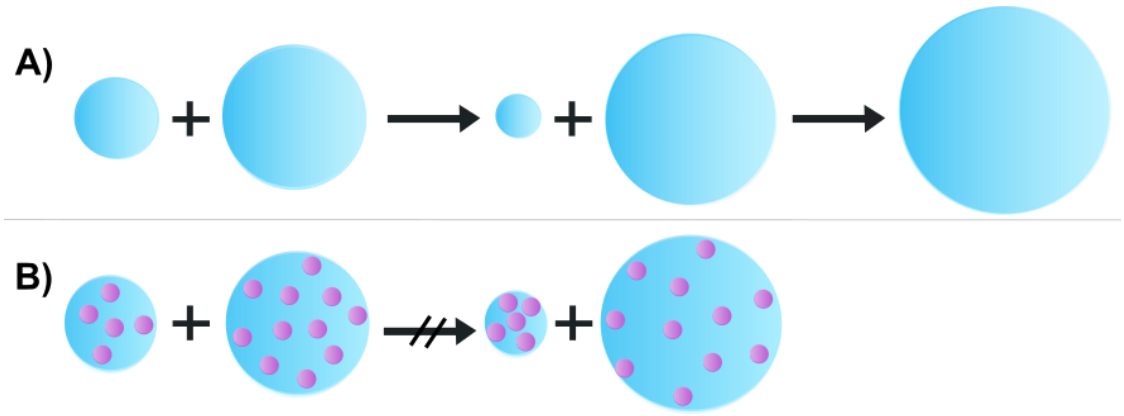

Figure 4: A) Scheme of progressing Ostwald ripening over time. **B)** Suppression of Ostwald ripening by adding an osmotic pressure agent (example: salt) to the polar dispersed phase.

As the resulting osmotic pressure inside the droplets is well below the Laplace pressure, no thermodynamic equilibrium state in which the Laplace pressure is identical to the osmotic pressure is created. Instead, the addition of the osmotic pressure agent stabilizes the miniemulsion by a state of equal effective pressure inside all droplets because the creation of a heterogeneous population of droplets would lead to a loss of free energy in comparison to a homogenous droplet size distribution. Therefore the droplets are in an equilibrium state and their size does not change over time, making the miniemulsion thermodynamically stable against Ostwald ripening.[22-23]

In conclusion, the miniemulsion process is a versatile and easily scalable technique that can be used for synthesizing a broad variety of organic and inorganic nanostructures while exceeding the possibilities of a regular emulsion polymerization that is limited to free radical polymerizations. Since it enables the encapsulation of different materials while also providing the means for functionalizing the obtained particles, it is a versatile tool for the synthesis of nanoparticles and nanocapsules as for example SiNCs.[24]

3.3 Silica nanocapsules (SiNCs)

As discussed previously, nanocapsules are hollow nanoparticles composed of a solid shell surrounding a cavity in which substances or active compounds can be enclosed. Due to this large inner cavity, nanocapsules offer the advantages of a high loading capacity and a low density while also exhibiting favorable colloidal properties.[25] Silica is considered a promising material for manufacturing these nanocapsules, especially for biomedical applications, as it is non-toxic and exhibits high biocompatibility. Besides these advantages, it is also mechanically and chemically stable, optically transparent, and cost-effective in production. Additionally, the surface of silica nanostructures has a high coverage with hydroxyl groups giving access to functionalizing the surface with a broad variety of different moieties such as antibodies, dyes, or polymers via siloxane chemistry as depicted in **Figure 5**.[4] Moreover, these hydroxyl groups make the SiNCs hydrophilic, which enhances their colloidal stability and water solubility.[26]

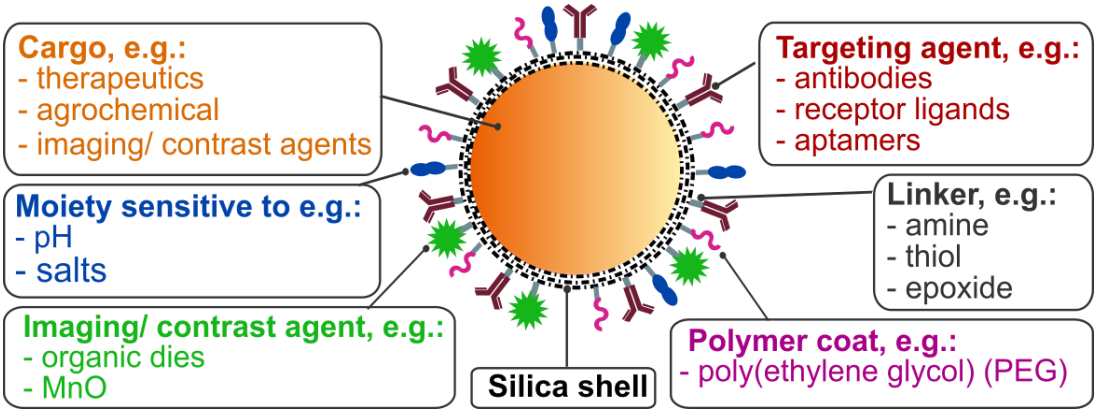

Figure 5: Schematic of a multifunctional, cargo-loaded, and stimuli-responsive SiNC.

When synthesizing silica-based nanocapsules, gaining control over the structural features of the capsules such as size, shell porosity, surface functionalities, and cavity topology is a non-negligible necessity. The size and size distribution are majorly controlled by the chosen synthesis method.[26] **Figure 6** shows the important steps of the synthesis of SiNCs. In the first step, a nano-sized template is prepared. Since the chemical and electrostatic affinity of the template's surface and the silica precursors must be favorable, the surfaces of some templates require an additional step of surface modification before deposing the silica shell onto the template in the next step. In the last step, the template is removed to obtain the desired capsule.[4]

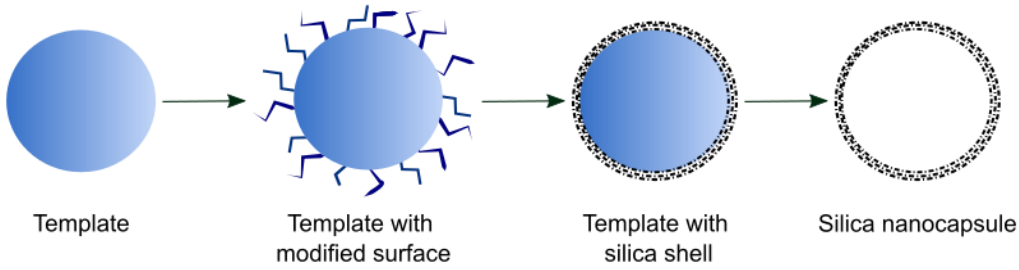

Figure 6: Schematic illustration of a conventional process for synthesizing hollow SiNCs.

In accordance with the employed template, the cavity-generating strategies are categorized as either hard or soft templating or template-free strategies. Hard templates are rigid templates such as inorganic nanoparticles or polymers, which have to be removed to obtain a hollow shell. Therefore, the shape and size of the cavity is dictated by the chosen template, leading to capsules with a well-defined morphology and a monodisperse size distribution.[27] Hence, a hard templating strategy is favorable for synthesizing monodisperse capsules in the size range below 100 nm. But major drawbacks of the hard templating approach are the limited options of accessible templates, the high effort required to remove the template, and the challenges faced with both in-situ encapsulation and post-loading of cargo inside the hollow cavity of the empty nanocapsules.[26]

On the other hand, flexible, oftentimes liquid or gaseous templates such as droplets, micelles, or gas bubbles are known as soft templates. But the capsules prepared by a soft template approach often suffer from high dispersity, ill-defined morphologies and usually exhibit broader size distributions. However, soft templates offer the subsequent advantages over hard templates: Firstly, the removal of soft templates is gentler than the harsh conditions used for removing hard templates via chemical etching or thermal calcination.[28] This makes a soft template approach oftentimes more economical, less time-consuming, and more environmentally friendly, waiving the use of toxic chemicals. Moreover, the challenging re-filling step can be avoided, as an in-situ encapsulation of different compounds inside the capsules is possible which further simplifies the synthesis. A commonly used soft templating synthesis method is the miniemulsion technique described in the previous section.[27]

Lastly, some new template-free strategies for the synthesis of hollow nanospheres have been developed. They are often based on Ostwald ripening and Zhang et al. established a kinetically controlled synthesis without sacrificial templates for hollow silica nanostructures with unusual morphologies, as for example rods and tubes.[29] Even though these template-free methods hold the potential to overcome some of the inherent obstacles of template-based strategies, they are less common and more limited in their

application than the well-established template based methods. Nonetheless, they offer a possibility to overcome incompatibility issues between the template and the deposition material, limit the excessive energy consumption and high costs of removing hard templates and gain control over the inhomogeneity and polydispersity of the nanocapsules synthesized via a soft templating approach. Overall, template-free strategies are preferably used in large-scale applications due to the simpler synthesis and the uncomplicated scale-up.[30]

In addition to the size and the size distribution, the morphology of the cavity inside the capsules is mainly determined by the used template as well. The cavity can either consist of a single compartment or of several single concentrically layered membranes, comparable to the structure of an onion. This cavity configuration has a direct impact on the loading capacity and the release behavior of the capsules.[26] The shape of the cavity can be tailored as well, even though the synthesis of non-spherical shapes like cubic structures still opposes a considerable challenge. In general, non-spherical templates are limited in their accessibility, because especially soft templates such as micelles or droplets have the tendency to form spherical shapes in order to minimize their interfacial energy. Additionally, there is also a scarcity of non-spherical hard templates. On top of this, the deposition of a uniform silica layer on a non-spherical surface is strenuous due to the pronounced differences in curvature.[27]

The porosity or density of the silica shell has to be controlled in order to control the diffusion of small molecules into and out of the hollow cavity. For bulk mesoporous materials the pore sizes can be varied using traditional surfactant structure-directing approaches, but they are often not suitable for manufacturing hollow spheres with large pores. Such larger pores in the size range above 10 nm can be achieved by a surfactant-directing alkaline-etching strategy.[31] When synthesizing the SiNCs via sol-gel chemistry, the amorphous shell contains micropores in the sub-nanometer range. However, since the permeability of these pure silica shells is not controllable, composite-type structures with an organic fraction for controlling the permeability can be beneficial. Especially for controlled release bio applications silica shells with a tunable pore size and a high porosity are desirable.[26] The synthesis of hollow SiNCs via sol-gel chemistry is the subject of the following section.

3.4 Sol-gel processes

A sol-gel process is a process in which liquid precursors progress into forming a sol and finally a gel. This means that the liquid precursors form a fluid colloidal system consisting of at least two, but possibly more components, which then evolves into a non-fluid colloidal or polymeric network whose entire volume is expanded by fluid. Afterwards, the obtained gel can be dried to obtain a dry network.[32] Even though metal alkoxides, organometallic precursors and metal cations are all suitable precursors for sol-gel processes, the following specifications will focus on traditionally used alkoxide-based precursors as e.g. tetramethyl orthosilicate $Si(OMe)_4$ (TMOS). Regardless of the desired application of the obtained material, a sol-gel process usually proceeds along the following steps: Firstly, a stable solution of the alkoxide precursors has to be formed. Secondly, polycondensation leads to the formation of an oxide-bridged network and induces gelation. Afterwards, the polycondensation reaction proceeds further which leads to the aging of the gel. Lastly, the gel can be dried by removing residual liquid from the gel network and optionally be stabilized against rehydration by calcination.[33]

In the course of these steps of the sol-gel process, silicon alkoxides have to undergo hydrolysis followed by a condensation reaction. Both steps are highly dependent on the chosen process parameters, such as the catalyst, its concentration, the ratio of alkoxide to water and the R-group present in the alkoxide. Since a sol-gel process at neutral pH is usually very slow, acid, base or fluoride are used as catalysts to accelerate the reaction. Depending on the chosen catalyst, the relative reaction rate of the hydrolysis in comparison to the rate of the condensation changes. This change in the ratio of the two rate constants (k_H/k_C), which accompanies the different reaction mechanisms, results in some significant changes in the structure of the silica gel.[34]

When employing acid as the catalyst the hydrolysis proceeds according to the nucleophilic substitution (S_N2) mechanism depicted in **Figure 7, A**. During hydrolysis, a hydroxyl group replaces one of the alkoxy groups. To achieve this, the alkoxy group is protonated rapidly which leads to the withdrawal of electron density from the silicon. Thereby, the electrophilicity of the silicon atom increases and makes it more susceptible to the nucleophilic attack by water. After passing through a pentacoordinate transition state, a hydrolyzed silicon alkoxide and the byproduct alcohol (ROH) are obtained. The base catalyzed hydrolysis depicted in **Figure 7, B** shares several similarities with the acid-catalyzed hydrolysis, as it passes through a pentacoordinate transition state when replacing one alkoxy with a hydroxyl group as well. But as the silicon alkoxide undergoes a nucleophilic attack by hydroxide, an alkoxide (RO^-) is eliminated as the byproduct.

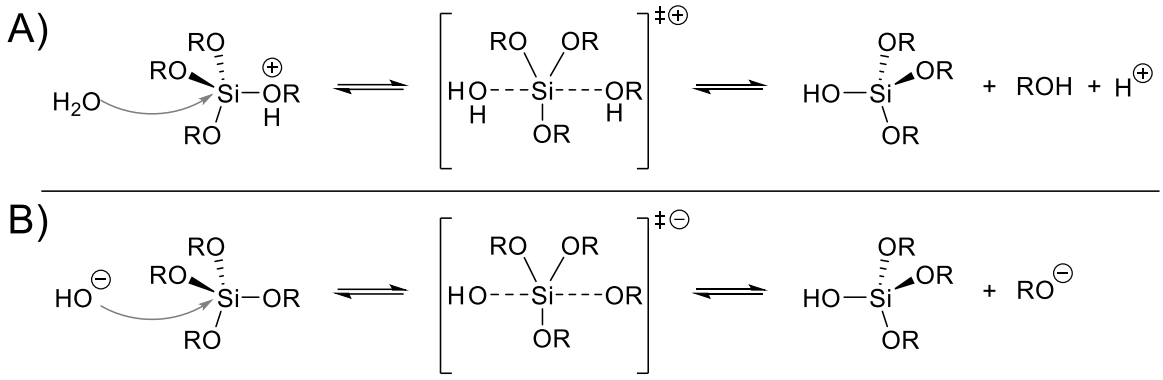

Figure 7: A) Acid catalyzed and B) base catalyzed hydrolysis of silicon alkoxides.

The condensation can be performed under both acidic (**Figure 8, A**) and basic conditions (**Figure 8**, **B**) and in both cases, at least one silanol group is required for the formation of the desired siloxane bond. Therefore, the proportion of silanol groups already obtained by hydrolysis influences the progress of the condensation reaction. Under acidic conditions, the hydrolysis rate decreases when substituents with increasing steric hindrance are attached to the silicon. On the other hand, electron-providing substituents increase the rate, as they stabilize the positive charges developed during the hydrolysis.[35] Therefore, the hydrolysis of the first alkoxide group is usually the fastest and the reaction rate decreases for each further hydrolysis of an additional –OR group.[34] Furthermore, condensation reactions may preferentially take place between a neutral species and a monomeric silanol or a silanol end group of a chain, because these silanols are the most basic and therefore most probable to get protonated. Overall, both the hydrolysis and the condensation reaction under acid catalysis facilitate the formation of a more linear and weakly cross-linked network as depicted in **Figure 9**.[35]

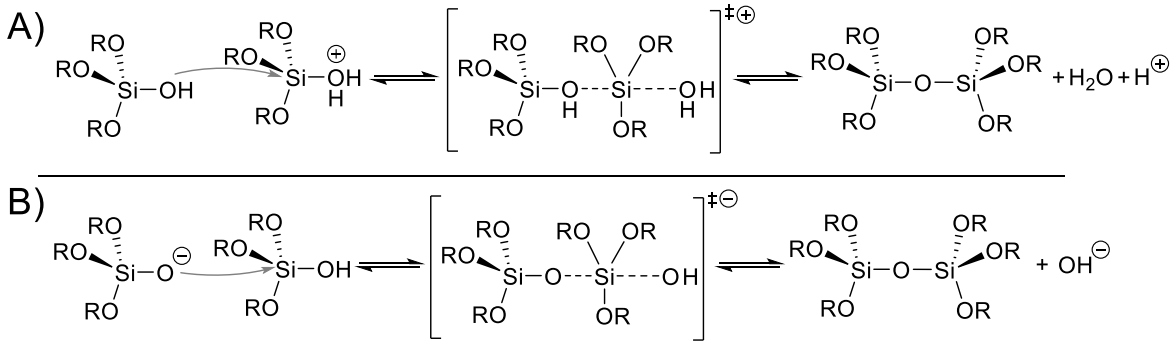

Figure 8: A) Acid catalyzed and B) base catalyzed condensation of silanols.

In contrast, base catalyzed hydrolysis and condensation lead to a highly branched network as shown in **Figure 9**.[36] One plausible cause for this is that electron-withdrawing substituents enhance the hydrolysis rate when using a base as the catalyst because they stabilize the negative charge. Hence, the hydrolysis rate increases with each alkoxide that is replaced by a silanol group. Moreover, the acidity of a silanol proton increases when

one of the other –OR or –OH groups linked to the same silicon atom is replaced by a more electron-withdrawing -SiO group. As this makes deprotonated silanols with siloxane bonds more accessible, a higher degree of crosslinking becomes more favorable.[35]

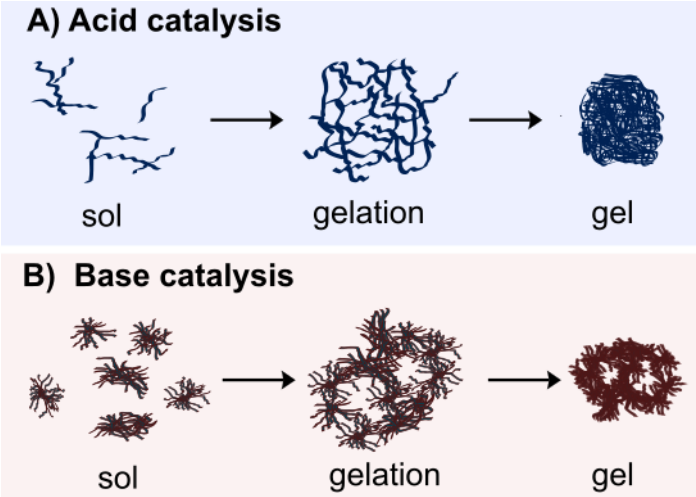

Figure 9: Scheme of the change of an inorganic structure from a sol to a gel with either acid (**A**) or base (**B**) as the catalyst.

Overall sol-gel processing is a versatile technique, that cannot only be employed for the fabrication of ceramics and glasses, but also for the fabrication of thin films, nanocomposites and nanoparticles. In 1968 Stöber et al.[37] developed a pioneering sol-gel process for the formation of silica particles in the size range of 50 nm to 2 µm. Their synthesis employed tetraethyl orthosilicate (TEOS) as the silica precursor and ammonia as a morphological catalyst[37] and until today the Stöber process is still widely used due to its advantage of being a surfactant-free method.[38] Recently, several sol-gel-based methods for the synthesis of SiNCs have been developed. For the capsule synthesis miniemulsions are commonly used as the sol-gel reaction can be constricted to occur only at the interface of the emulsion droplets. It is possible to synthesize SiNCs with both organic and aqueous cores with the miniemulsion technique, but only the synthesis of SiNCs with an aqueous core via sol-gel chemistry will be discussed here.

The reported methods for synthesizing SiNCs with an aqueous core differ mainly in the employed surfactants, the used silica precursors and the catalyst used. One method uses the interactions between the positively charged surfactant cetyltrimethylammonium bromide (CTAB) and the under basic conditions negatively charged silica species, which is obtained through the hydrolysis of TEOS, to constrict the sol-gel reaction to the interface of the droplets in an inverse miniemulsion.[39] A different technique uses the interfacially active silica precursors (3-aminopropyl)trimethoxysilane (APTMS) and octyl trimethoxysilane to confine the sol-gel process at the interface while using either ammonia or fluoride as a catalyst to obtain capsules in the size range of 600 nm.[2]

As depicted in **Figure 10**, the sol-gel reaction can also take place without the addition of an external catalyst like fluoride or ammonia. Instead, it can be catalyzed by the (3-aminopropyl)triethoxysilane (APTES) precursor, which accumulates at the droplet interface in an inverse miniemulsion. One possible reason for APTES catalyzing the hydrolysis which is initiated upon contact of the added precursors with the water phase is the basic localized pH at the interface because of the higher concentration of amine functionalities at the interface. With this suggested mechanism the bulk pH remains neutral, making this synthetic strategy an elegant method for limiting the sol-gel process to the interface when encapsulating pH-sensitive molecules or enzymes.[5]

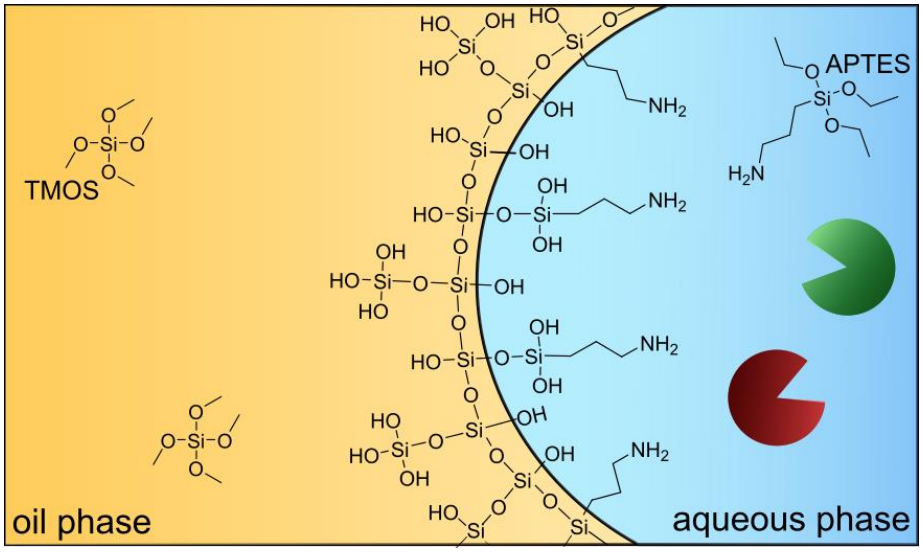

Figure 10: Interfacial sol-gel process in an inverse miniemulsion of silica precursors to form hollow nanocapsules.

3.5 Enzymatic nanoreactors

As described in the previous section, enzymes can be encapsulated inside of SiNCs that are synthesized by an interface confined sol-gel process. These enzyme-loaded SiNCs are then referred to as enzymatic nanoreactors, as the encapsulated enzymes catalyze a reaction in a confined nano-environment. While enzymatic nanoreactors in general can be designed for various applications as for example prodrug activation in cancer therapy,[40] one aspiring field of application is the use of enzymatic nanoreactors as synthetic organelles for synthetic cells.[5]

One of the core statements of cell theory is that every cell is created from another living cell by cell division since there is no knowledge of how the first cells were created from non-living components. Nonetheless, this process must have occurred at least in one instance in order to create the very first cell. Currently designing artificial, simplified cell-like model systems is viewed as a feasible approach to gain a better understanding of the origin of the first cells and thereby the origin of life.[41]

In general, living organisms are very complex and so is synthesizing them in a bottom-up approach from scratch, because artificial cells should exhibit at least some characteristics of living cells as for example the ability to self-reproduce and metabolize.[1] But for minimal artificial cellular systems the initial and most fundamental condition is compartmentalization, as nearly all life processes take place in compartments. Compartmentalization enables living systems to operate far from the thermodynamic equilibrium.[41] It separates different chemical micro-environments and introduces a semipermeable boundary that helps to protect the compartmentalized micro-environments against the changing external conditions, which is necessary to sustain all living systems.[42]

As depicted in **Figure 11**, semipermeable micro- and nanocapsules that encapsulate enzymes are model systems for compartmentalization and can be used to mimic cell organelles for the design of artificial cells.[1] In comparison to the use of free enzymes, encapsulating the enzymes inside of nanocapsules offers considerable advantages. Firstly, the design of specialized nanocapsules as compartments can be employed to both localize compatible enzymes for cascade reactions in one compartment or to separate non-compatible enzymes by encapsulating them inside different compartments.[42] This enables favorable cascade reactions to proceed more efficiently because intermediates can be enriched inside the compartment and spatial proximity of the enzymes for the subsequent reaction steps is ensured. Secondly, all compartments have to be surrounded by a semipermeable barrier, which confines the enzymes inside but allows the diffusion of the substrates and products. This semipermeable barrier also increases the stability of the

enzymes by protecting them against the interaction with proteases or toxic chemicals, thus creating a favorable micro-environment for the enzymes.[43]

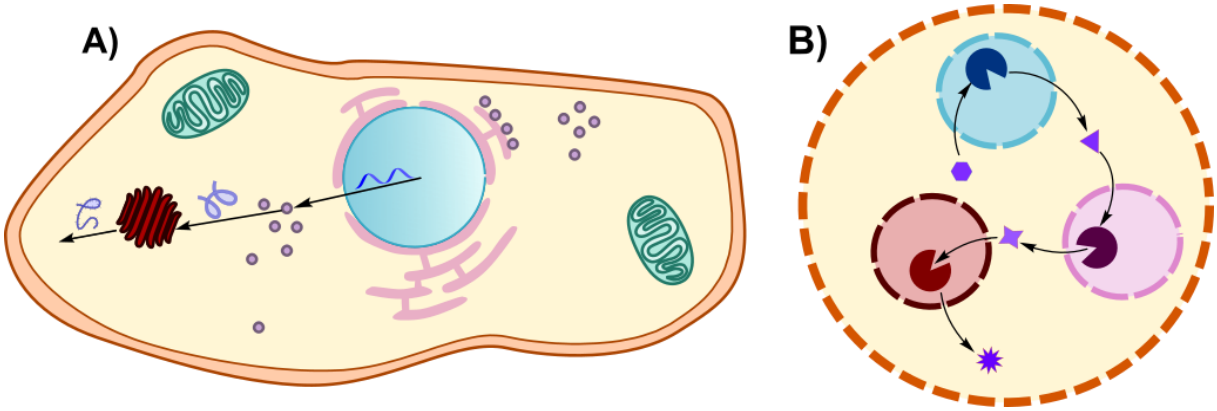

Figure 11: Comparison of a cascade reaction between the compartmentalized organelles of **A)** a simplified eucaryotic cell and **B)** an artificial cell-like system consisting of enzymes confined in nanocapsules (nano-organelles) inside a micro-confinement.

On the other hand, the design of artificial compartments faces considerable obstacles such as the inhibition of the enzymes by the accumulation of product or intermediate inside the capsules[44] and the difficulty to achieve an efficient loading of the compartments with enzymes. Finetuning the material for the nanoreactor can help to overcome these challenges and there is a broad pool of materials to choose from as for example vesicles prepared from amphiphilic copolymers or phospholipids or SiNCs.[45]

Enzyme-loaded SiNCs with an aqueous core are optimal candidates for enzymatic nanoreactors as they can encapsulate a wide range of enzymes with a remarkable efficiency at room temperature. Moreover, their synthesis does not form byproducts that might inhibit the enzyme and they can be synthesized in a one-step procedure.[2] In recent advancements, Jo et al.[46] successfully demonstrated that enzyme-loaded silica nanoparticles can be used as sub-compartments in aqueous micro confinement. They mimicked the triple cascade reaction of β-glucosidase, glucose oxidase, and horseradish peroxidase and showed that reactions between the nanoconfinements are possible, while the introduced silica shell offers additional protection for the enzymes against proteolytic degradation and heat.[46] Additionally, Jiang et al.[5] described an in-situ encapsulation approach for loading enzymes on silica nanocapsules instead of silica nanoparticles. It was demonstrated that competitive cascade reactions can be regulated by co-encapsulating different enzymes within the same SiNC. Moreover, the silica nanoreactors were incorporated inside of polymer vesicles to function as artificial organelles within multicompartmentalized synthetic cells.[5]

In conclusion, SiNCs are a promising platform for the synthesis of synthetic, enzyme-loaded nano-organelles, that can be used to study the effects of compartmentalization. Thereby, they contribute to the efforts of designing artificial cells and they might be useful as artificial organelles for the incorporation into living cells in the future.[5]

4. Results and Discussion

4.1 Optimization of the SiNC synthesis in small volumes

The procedure for synthesizing SiNCs described by Jiang et al.[5] was used as the starting point for developing the synthesis strategy for SiNCs in small quantities. As optimizing the enzyme encapsulating nanocapsules requires testing numerous different enzyme concentrations and ratios, downscaling the original synthesis is desirable to reduce the required quantities of enzyme and silica precursors. Moreover, a reduction of the total volume of the reaction mixture is accompanied by a decreased volume of the dispersed phase in which the enzymes are dissolved before emulsification, which enables studying a broader range of enzyme concentrations using the same absolute amount of enzyme.

Similar to the original procedure the capsules were prepared in an inverse (water-in-oil) miniemulsion. The enzymes were pre-dissolved in the aqueous phase in order to encapsulate them directly into the aqueous core of the SiNCs during the formation of the silica shell. As depicted in **Figure 12**, polyglycerol polyricinoleate (PGPR) was used as the low HLB surfactant for stabilizing the inverse miniemulsion. TMOS and APTES were used in a 5.5:1 molar ratio as the silica precursors. The high HLB surfactant Lutensol AT50 was employed when transferring the formed capsules to water. As Lutensol-AT 50 is a PEG-based and neutral surfactant, it has the ability to increase the stability of nanocapsules in biological media.[47]

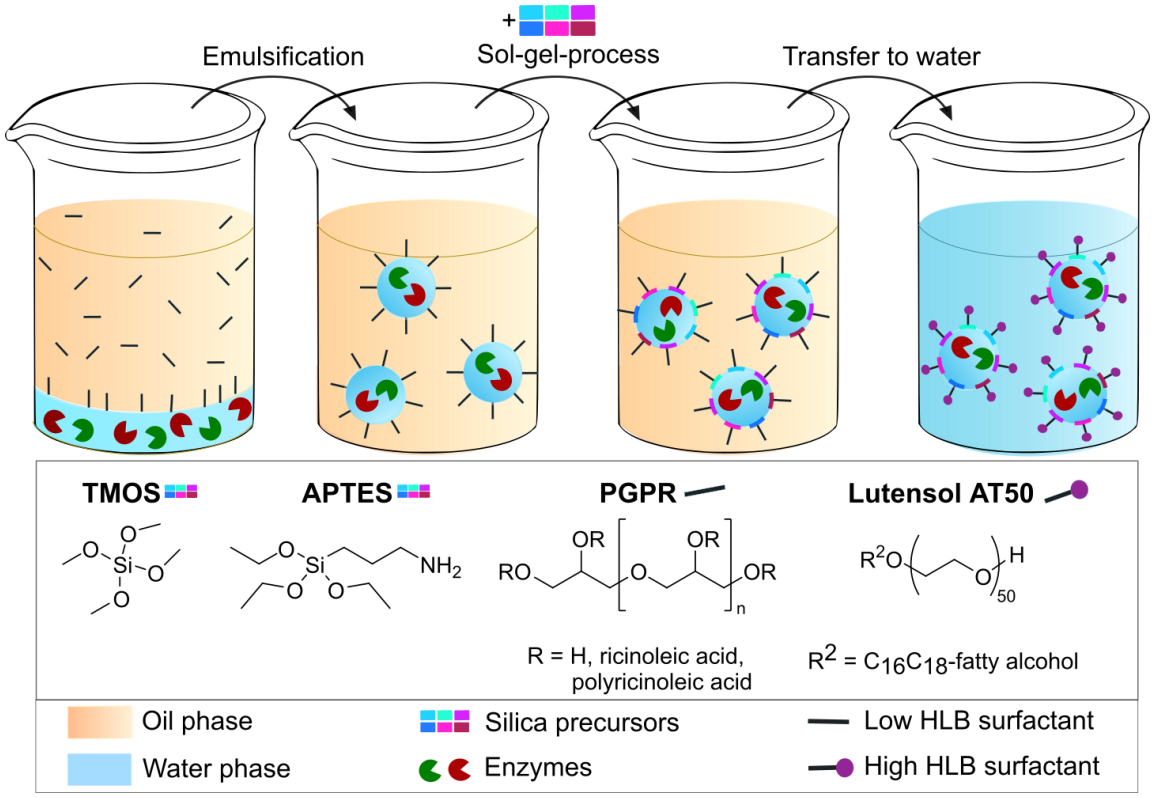

Figure 12: Schematic illustration of the synthetic procedure for preparing the in situ loaded SiNCs using an inverse miniemulsion technique before transferring the capsules to aqueous medium.

In comparison to the original procedure, the volumes of the continuous and the dispersed phase were reduced by two-thirds for downscaling. Therefore, the LM10 Microfluidizer® used in the original procedure was no longer suitable as it can only process emulsion with a minimum volume of 30 mL. The evaluation of both ultrasonication and high-pressure homogenization with a small-volume LV1 Microfluidizer® for the preparation of the miniemulsions is the subject of the first subsection. The testing of different reaction times and options for the precursor addition will be discussed in the following subsection, before discussing the influence of the silica precursors on the capsule morphology. Moreover, the use of an alternative low HLB surfactant for the miniemulsion fabrication will be assessed.

4.1.1 Comparison of emulsification techniques

In order to establish the optimal emulsion processing technique for small volumes, high-pressure homogenization and sonication were used to fabricate various emulsions. Overall, all parameters in the SiNCs-preparation besides the chosen emulsion processing technique were identical to ensure comparability.

The inverse miniemulsion consisted of cyclohexane as the continuous phase, Dulbecco´s sodium phosphate buffer (DPBS) as the dispersed phase and PGPR as the low HLB surfactant. At first, empty SiNCs without any enzyme were fabricated. Before processing, the two phases were stirred and afterwards homogenized with an UltraTurax T18 dispersion unit.

For emulsification the samples were sonicated for a total of 180 s (20 s ultrasonication, 10 s pause) at 30% amplitude with a Branson 450W sonifier with a 1/2´ tip under ice cooling. Depending on the employed processing technique, the capsules will be referred to as son-SiNCs when sonication or as hph-SiNCs when high-pressure homogenization was chosen for emulsification. After emulsification, the obtained emulsions were divided into samples of 3 mL each before adding the silica precursors to ensure reproducibility of the capsule formation by having at least two similar samples. The obtained capsules were characterized using dynamic light scattering (DLS) and transmission electron microscopy (TEM) micrographs. For synthesizing empty SiNCs, two emulsions were separately fabricated with each of the two processing methods. These four emulsions were then characterized by DLS, the obtained droplet sizes and polydispersity indices (PDIs) are displayed in **Table 1**.

Table 1: Hydrodynamic diameters and PDIs of the emulsion droplets synthesized using either sonication or high-pressure homogenization as the emulsification technique measured in cyclohexane.

Emulsion	Sonication		High-pressure homogenization	
	d_h [nm]	PDI	d_h [nm]	PDI
A	221	0.42	228	0.15
B	289	0.48	234	0.17

When comparing the quality of the emulsions created with either the small volume LV1 Microfluidizer® or the sonication-tip, the emulsions fabricated by sonication exhibit a more than two times higher polydispersity than the emulsions obtained by high-pressure homogenization. Moreover, the size of the droplets obtained by high-pressure homogenization shows better reproducibility with 231 nm as the average diameter compared to 255 nm when using sonication. The hydrodynamic diameters and polydispersity indices of the SiNCs, that were synthesized from the afore described emulsions are listed below in **Table 2**.

Table 2: Hydrodynamic diameters and PDIs of SiNCs synthesized using either sonication or high-pressure homogenization measured in cyclohexane.

Sample	son-SiNCs			hph-SiNCs		
	d_h [nm]	PDI	emulsion	d_h [nm]	PDI	emulsion
1	238	0.26	A	286	0.24	A
2	251	0.28	A	298	0.24	A
3	251	0.26	A	336	0.18	B
4	284	0.40	B	-	-	-
5	224	0.24	B	-	-	-
6	224	0.27	B	-	-	-

Even though the difference in the PDIs of the son-SiNCs and the hph-SiNCs decreases - with 0.28 as the average for the son-SiNCs and 0.20 as the average for the hph-SiNCs - hph-SiNCs continue to exhibit a narrower and therefore more favorable size distribution. The capsules obtained after sonication are about 20% smaller than the capsules obtained after high-pressure homogenization as the son-SiNCs have an average size of 245 nm in comparison to 306 nm for the hph-SiNCs. Two exemplary DLS-graphs depicted in **Figure 13** show, that despite having identical average PDIs, the overall size distribution is more homogenous for the capsules derived from the emulsion processed with the LV1 Microfluidizer®.

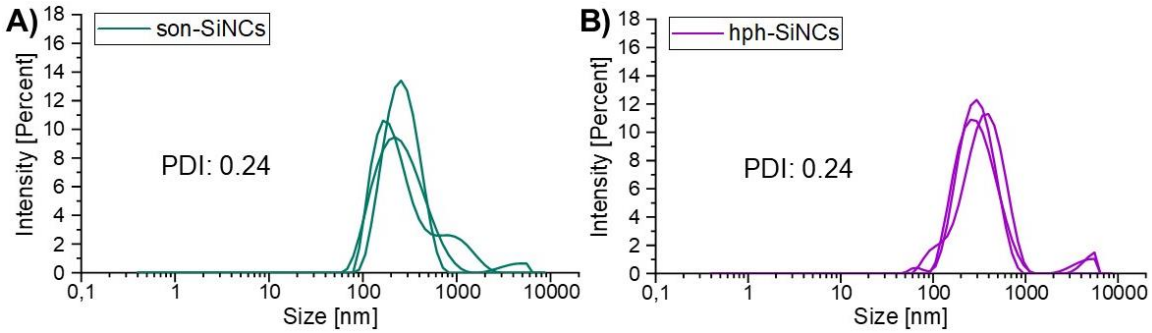

Figure 13: DLS graphs of the three measurement runs of **A)** SiNCs fabricated using sonication and **B)** SiNCs fabricated using high-pressure homogenization.

The TEM micrographs of the hgh-SiNCs in **Figure 14** show distinct capsules with an evident difference in contrast between the darker capsule shell and the inner cavity of the capsules. All capsules exhibit a spherical or near-spherical shape and range from about 100 nm to approximately 400 nm in diameter, which is in satisfactory agreement with the DLS measurements. In comparison to this, the son-SiNCs depicted in the TEM micrographs in **Figure 15** are not uniform with clearly visible disruptions in their shells. The contrast between the inner cavity and the shell is less pronounced and a high degree of deformation of the desired spherical shape can be observed. Moreover, a high number of structures without a distinct shell in the size range below 50 nm is visible in both TEM micrographs in **Figure 15**.

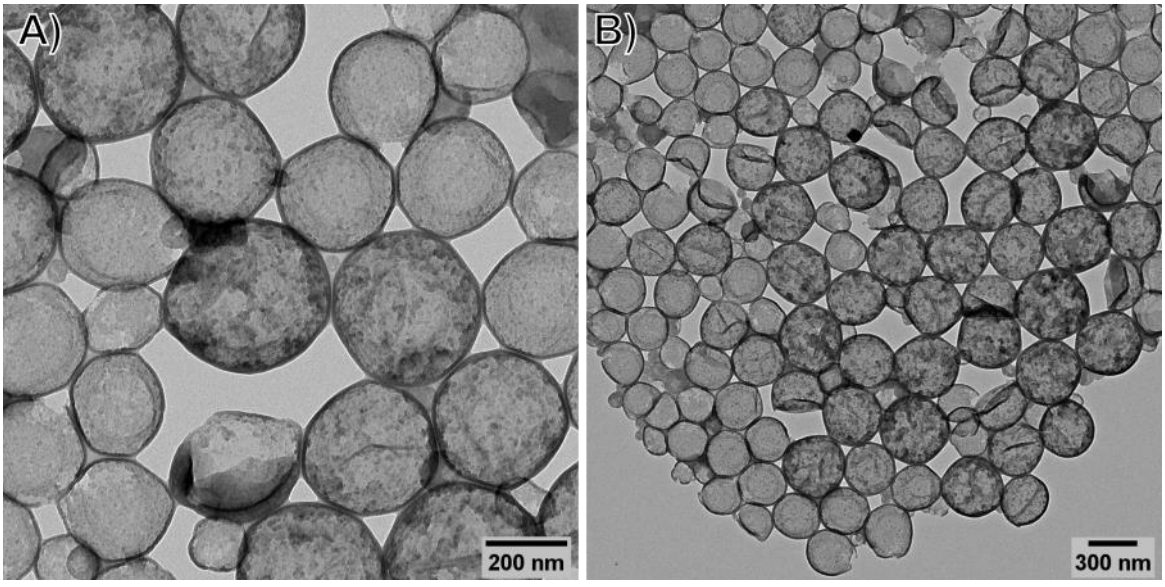

Figure 14: TEM micrographs of SiNCs fabricated from a high-pressure homogenized emulsion without encapsulated enzymes in cyclohexane.

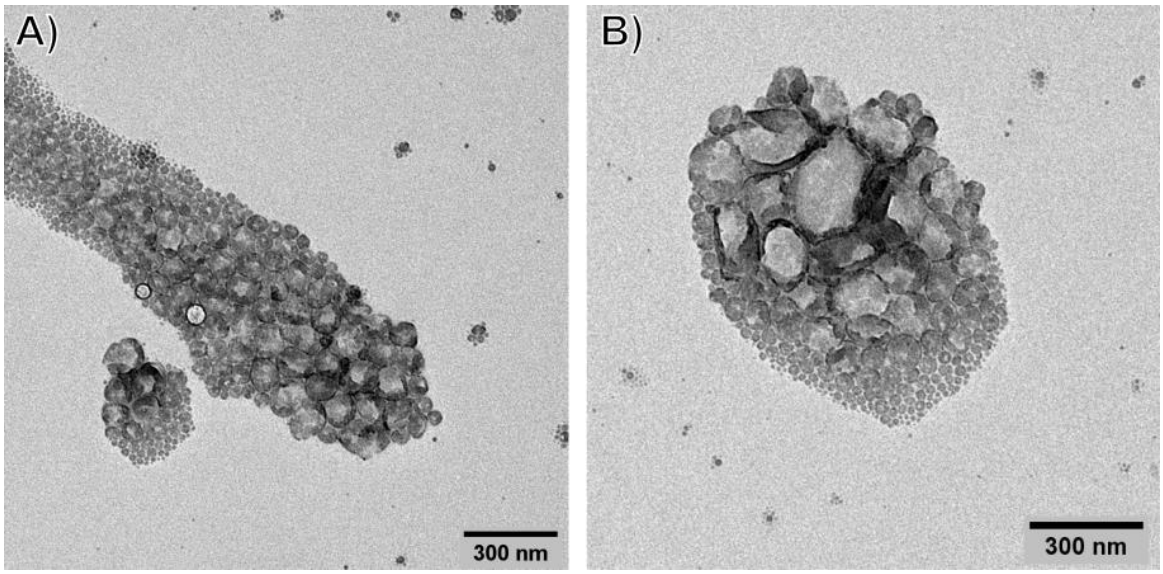

Figure 15: TEM micrographs of SiNCs fabricated from a sonicated emulsion without encapsulated enzymes in cyclohexane.

Due to the lack of distinct continuous shells in the TEM micrographs of the son-SiNCs, the thickness of the silica shells was only determinable for the hph-SiNCs. The percentage of the respective hph-SiNCs with a certain shell thickness is plotted against the respective shell thicknesses in **Figure 16**. It can be observed that shells with a thickness in the range of 10 – 14 nm make up more than 50% with nearly 37% of the remaining capsules having thicker and about 12% having thinner shells. Therefore, the average shell thickness of the hph-SiNCs is with 13.4 ± 3.3 nm significantly lower than for APTMS/TEOS-SiNCs synthesized under basic catalysis which exhibit shells with an average thickness of 31 ± 6 nm.[2] This thinner shell might cause the obtained capsules to be less stable, which can lead to complications when transferring the capsules to aqueous medium.

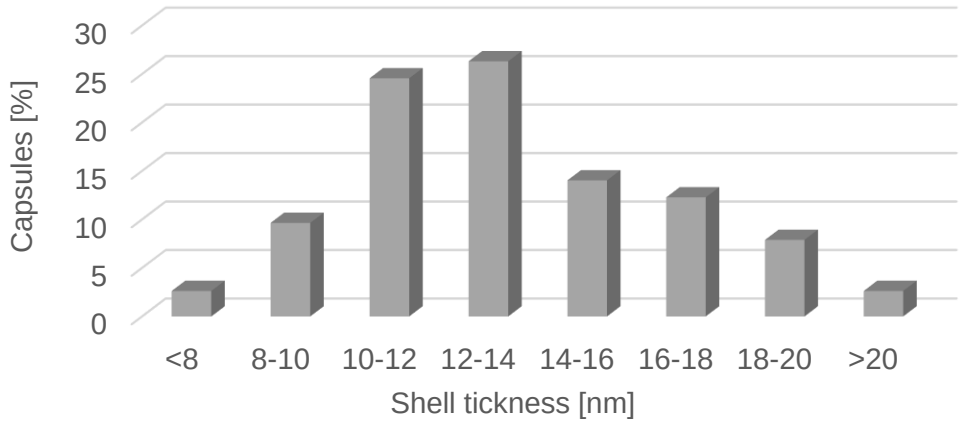

Figure 16: Shell thickness of SiNCs obtained after high-pressure homogenization of the emulsion. The thickness of the SiNCs was measured at 111 different points on the shells of various capsules using the measuring tool in ImageJ.

The transfer of the SiNCs to aqueous medium employed Lutensol AT50 as a neutral surfactant, which helps to stabilize the nanocapsules in biological media. A successful

transfer could not be achieved for the son-SiNCs, as the aggregation of the nanocapsules could be observed while redispersing the capsules in aqueous medium. As shown by the results of the DLS measurements in **Table 3**, the hydrodynamic diameters of the son-SiNCs increased up to 1113 nm in water and the polydispersity increased drastically. A plausible reason for this is the incomplete shell formation observed in the earlier described TEM images. The high stress acting on the nanocapsules during redispersion in the sonication bath could lead to the destruction of the unstable, incompletely formed SiNCs and subsequent aggregation of the individual shell fragments. As shown in the appendix in **Figure 36**, macro-sized aggregates could be observed by the naked eye after redispersion.

Table 3: Hydrodynamic diameters and PDIs of SiNCs synthesized using either sonication or high-pressure homogenization for emulsification measured in water.

Sample	son-SiNCs		hph-SiNCs	
	d_h [nm]	PDI	d_h [nm]	PDI
1	468	0.59	375	0.37
2	513	0.47	461	0.37
3	1113	0.46	369	0.41

Considering the hph-SiNCs, an increase in the diameter was observed as well, but due to the thicker, more stable shells, the hph-SiNCs are more protected against breakage due to swelling than the son-SiNCs. Nonetheless, the obtained PDIs show a considerable increase in the dispersity which could be caused by some degree of aggregation as well. An optimization of the redispersion to prevent the size and polydispersity from increasing was still necessary and will be part of section 4.2.

In order to study if the presence of the to be encapsulated enzyme influences the morphology of the SiNCs, GOx@SiNCs with three different GOx concentrations were synthesized using both sonication and high-pressure homogenization. The TEM micrographs in **Figure 17** showed similar morphologies for the GOx@SiNCs with both high and low concentrations of GOx when sonication was used. It was concluded that the impact of GOx on the shell formation is neglectable for the son-SiNCs and will not be discussed to any further extent. The results for the GOx@SiNCs produced with high-pressure homogenization are presented in section 4.3.

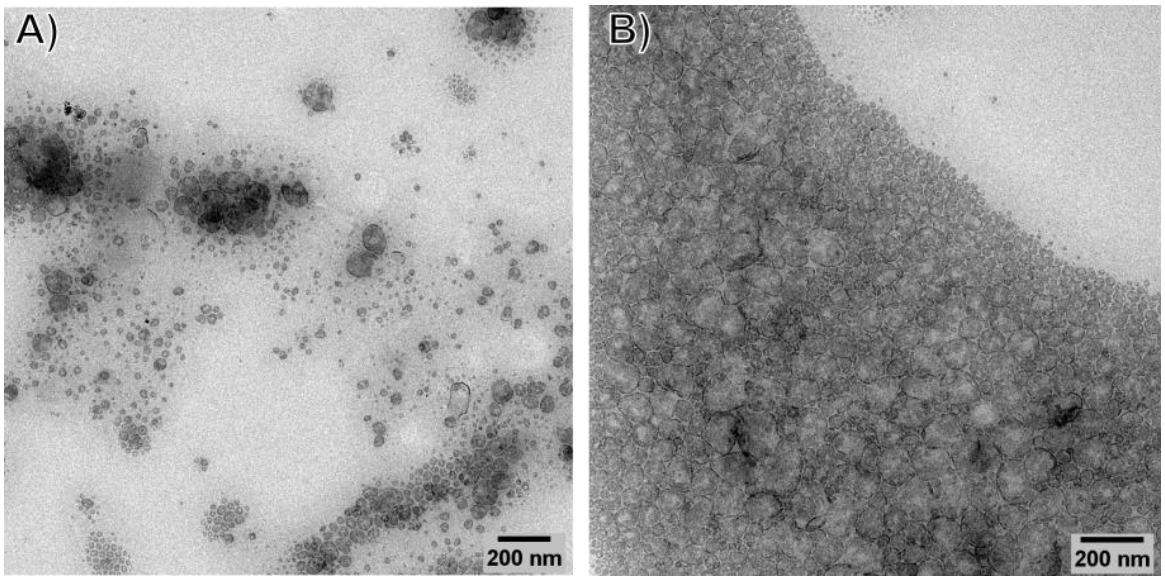

Figure 17: TEM micrographs of GOx@SiNCs synthesized with sonication as the emulsification technique with **A)** 10 mg/mL and **B)** 1 mg/mL as the GOx concentration in the dispersed phase measured in cyclohexane.

In conclusion, high-pressure homogenization with the LV1 small-volume Microfluidizer® was established as the preferable method for processing miniemulsions when synthesizing SiNCs. The obtained emulsions exhibited lower dispersities and enabled the formation of uniform and continuous shells.

4.1.2 Optimization of the precursor addition and reaction time

Different procedures for adding the silica precursors TMOS and APTES to the miniemulsion were investigated in order to study their impact on the capsule size and dispersity. For this purpose, two different emulsions were prepared using the afore established high-pressure homogenization. The droplet sizes of both emulsions were comparable with 209 nm and 231 nm, making the emulsions suitable for setting up three different syntheses. The three syntheses differed only in the precursor addition, not in the total amount of precursors used. When synthesizing the first batch (SiNCs A), TMOS and APTES were added separately to the emulsion. In contrast, the two precursors were pre-mixed before adding them to the second batch (SiNCs B) and a solution of TMOS and APTES in 1 mL of cyclohexane with PGPR (13.3 mg/mL) was employed in the synthesis of the third batch of capsules (SiNCs C). As listed in **Table 4**, the SiNCs A and B were both in the desired size range with 341 nm and 323 nm, while the addition of the precursors in cyclohexane resulted in SiNCs of nearly double this size with 609 nm. As the PDI of the capsules that were synthesized by adding the TMOS-APTES-mixture to the emulsion was the lowest with 0.13 and since this addition method is also the simplest with the least variables, it was used for all forthcoming synthesis.

Table 4: Hydrodynamic diameters and PDIs of emulsion droplets used for the preparation of SiNCs and of the SiNCs themselves measured in cyclohexane. * 3 mL of Emulsion B were stirred for 20 h without the addition of any precursor as a control.

Sample	d_h [nm]	PDI	Emulsion	Precursor addition
Emulsion A	231	0.22	–	–
Emulsion B	209	0.16	–	–
Emulsion B*	183	0.08	B	–
SiNCs A	341	0.25	A	TMOS & APTES separately
SiNCs B	323	0.13	B	TMOS-APTES-mixture
SiNCs C	609	0.55	B	TMOS-APTES-mixture in C_6H_{12}

Irrespective of the addition method used, the formation of a white precipitate was observed in all three samples. For comparison, a portion of emulsion B was stirred for several hours without adding any silica precursors. Since precipitation was not observable without the addition of TMOS and APTES, the precipitate has to be formed by a reaction of the silica precursors.

Regarding the reaction time, the precipitate formation was already visible after two hours, and no alteration of the SiNCs-dispersion was observable by eye after less than 5 h of

stirring. As a result, the stirring time was reduced to 4 – 5 h and DLS measurements of the SiNCs were conducted. While the emulsion droplets were 236 nm in size with a PDI of 0.28 the two batches of SiNCs were 311 nm and 307 nm in size with PDIs of 0.10 and 0.05. Due to these promising results, TEM micrographs of the capsules were measured, and the capsules shown in **Figure 18** exhibit completely formed shells with an average thickness of 8.6 ± 2.4 nm. Therefore, the reaction time was reduced to 4 – 5 h for all following syntheses.

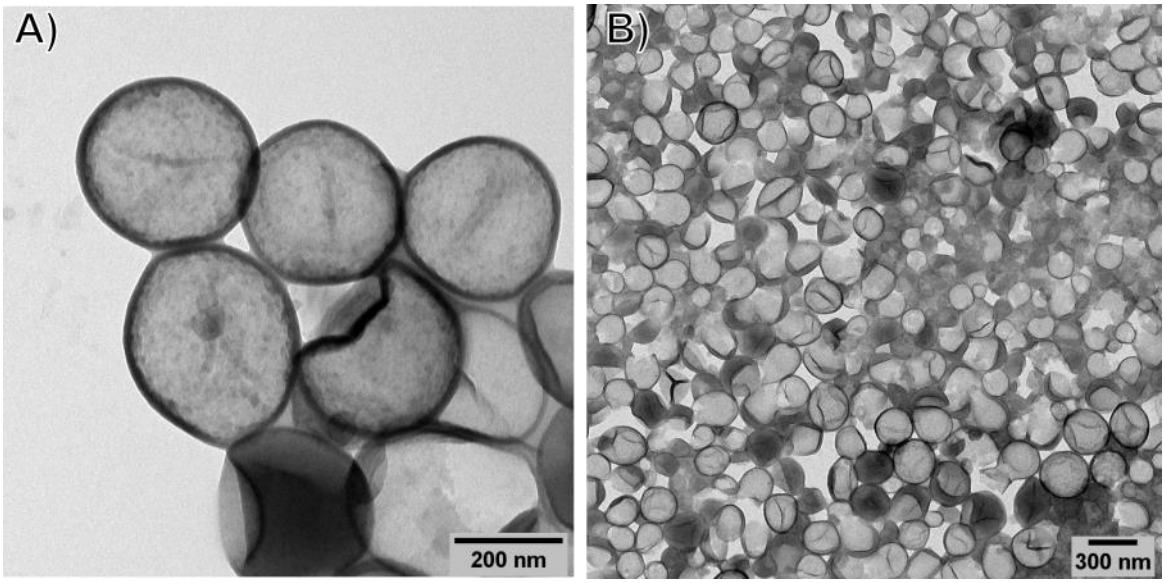

Figure 18: TEM micrographs of the SiNCs in cyclohexane after 5 h of reaction time.

4.1.3 Optimization of the silica precursors

When testing a different silica alkoxide and varying the amount of the employed silica precursor mixture, the main aim was to prevent the formation of the precipitate. The formation of a white solid, which is insoluble in cyclohexane, DCM, and water and precipitated at the bottom of the dispersion was observed in all priorly conducted synthesis approaches. As it only occurs when the silica precursors TMOS and APTES are added to the emulsion, the precipitate formation reduces the amount of silica precursors accessible for the shell formation. This makes gaining precise control over the shell thickness challenging. Hence, different attempts on optimizing the synthesis in order to prevent the precipitate formation were undertaken.

Overall, the sol-gel reaction takes place without the addition of an ancillary external catalyst, because the addition of an acid or base as the catalyst might damage the encapsulated enzymes and reduce their activity, due to changes in the secondary structure of the enzymes. While fluoride catalysis does not alter the secondary structure of the enzyme,[3] employing fluoride can pose a challenge because no trace of fluoride should be detectable in the finished nanocapsules. But as sol-gel reactions are usually not taking

place at a neutral pH, APTES is used as an additional precursor with TMOS. APTES is expected to accumulate at the interface of the aqueous droplets and oily phase, thus shifting the local pH at the interface towards a more basic level due to the high local concentration of amine groups. This suspected mechanism, constricting the sol-gel reaction at the interface, requires the use of a silica precursor with a high reactivity such as TMOS. On the other hand, the fast hydrolysis of TMOS was suspected to be a possible cause for the precipitate formation, due to the formation of silicon dioxide via complete hydrolysis instead of forming silica shells via polycondensation. In an attempt to reduce the precipitate formation, TEOS was tested as an alternative precursor to TMOS.

The same high-pressure homogenized emulsions, whose droplet sizes and polydispersities are listed in **Table 5**, were used for the fabrication of the nanocapsules with both precursors. The molar ratios of TMOS:APTES and TEOS:APTES were 5.5:1 and the same reaction times and reaction conditions were employed. When using TEOS as a substitute precursor for TMOS no precipitation was observed during or after the reaction.

Table 5: Hydrodynamic diameters and PDIs of the emulsion droplets after high-pressure homogenization measured in cyclohexane.

Emulsion A		**Emulsion B**	
d_h [nm]	**PDI**	**d_h [nm]**	**PDI**
228	0.15	234	0.16

The results of the DLS measurements listed in **Table 6** show, that the TMOS-SiNCs are overall slightly larger than the TEOS-SiNCS with an average hydrodynamic diameter of 306 nm in comparison to 284 nm. With an average PDI of 0.10, the TEOS-SiNCs exhibit a narrower size distribution than the TMOS-SiNCs with 0.16, with both average PDIs being in the desired range.

Table 6: Hydrodynamic diameters and PDIs of SiNCs fabricated with either TEOS or TMOS with APTES as the silica precursors measured in cyclohexane.

Sample	**TEOS**			**TMOS**		
	d_h [nm]	**PDI**	**emulsion**	**d_h [nm]**	**PDI**	**emulsion**
1	311	0.10	A	286	0.24	A
2	268	0.11	B	298	0.24	A
3	271	0.09	B	336	0.18	B

Even though the hydrodynamic diameters and PDIs of the TMOS-SiNCs and the TEOS-SiNCs are comparable, the TEM micrographs depicted in **Figure 19** and **Figure 20** show

fundamental differences in the morphologies of the nanocapsules. The TEM micrographs of the TMOS-SiNCs show spherical or near-spherical distinct capsules, with a high contrast between the shell and the inner cavity.

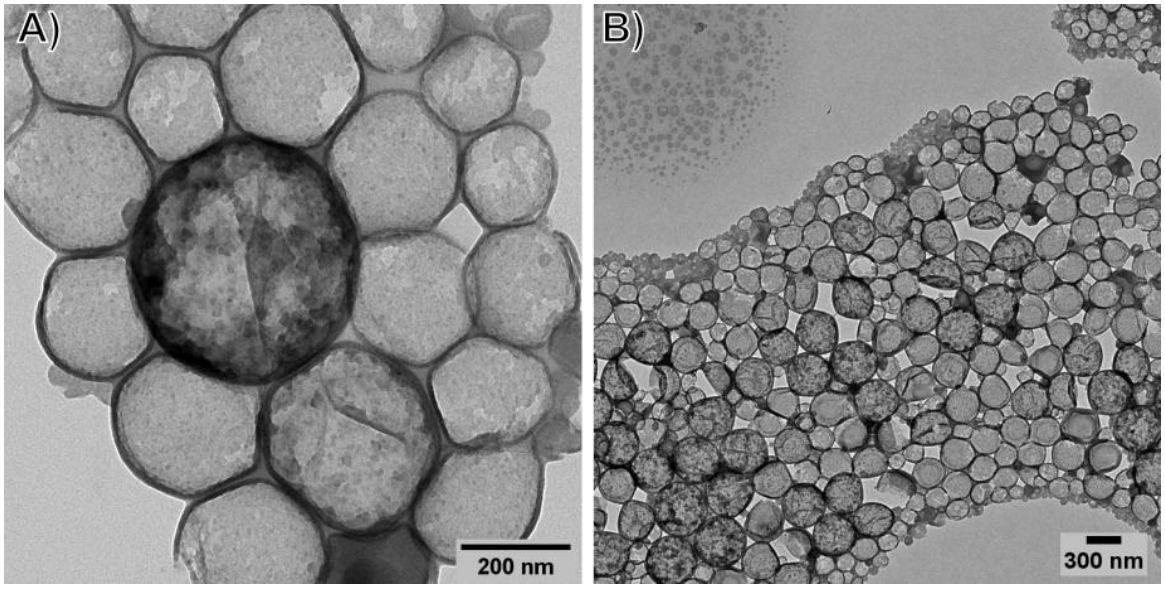

Figure 19: TEM micrographs of SiNCs fabricated with TMOS and APTES as the silica precursors without encapsulated enzymes in cyclohexane.

On the other hand, in the TEM micrographs of the TEOS-SiNCs no distinct capsular structures can be identified due to a lack of contrast between an inner cavity and a continuous shell. Many of the observable spherical structures are in a size range below 100 nm and the visible shell fragments are thinner than the intact shells of the TMOS-capsules. The incomplete shell formation with TEOS shows, that TEOS is not hydrolyzed fast enough to form a continuous shell without any additional catalyst present.

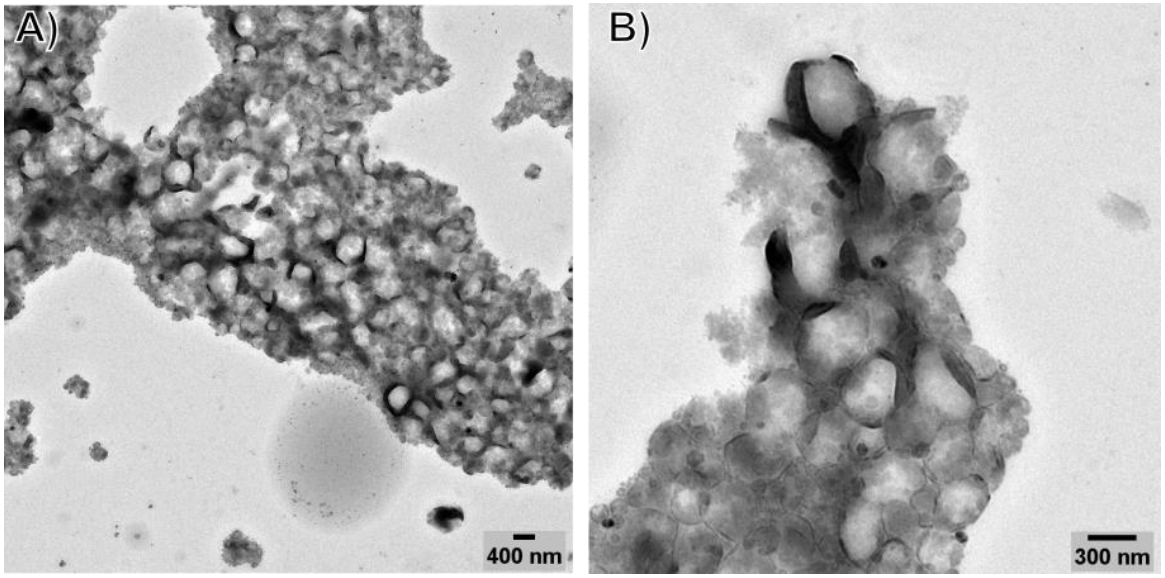

Figure 20: TEM micrographs of SiNCs fabricated with TEOS and APTES as the silica precursors without encapsulated enzymes in cyclohexane.

As replacing TMOS with a less reactive silica precursor led to an incomplete shell formation, the absolute amount of silica precursors was reduced to determine if excess silica not required for the shell formation facilitated the precipitate formation. **Table 7** displays the amount of silica precursors tested as well as the hydrodynamic diameter and PDI obtained by DLS measurements and the masses of the formed precipitate and the solid content of the supernatant.

Table 7: Volumes of added precursor mixture of TMOS and APTES and their relative percentage in comparison to the volume used in the original procedure. The hydrodynamic diameters and PDI of the capsules in cyclohexane are given as well as the mass of the precipitate formed and the solid content (SC) of the dispersion after removing the precipitate by centrifugation.

Sample	$V_{Precursor}$ [µL]	Percentage	d_h [nm]	PDI	m_{precip} [mg]	SC_{supern} [mg/mL]
1	15	33.3%	289	0.12	6	14
2	25	55.5%	266	0.13	11	16
3	30	66.6%	296	0.01	11	18
4	35	77.7%	299	0.01	10	22
5	40	88.8%	302	0.08	12	20
6	45	100%	296	0.09	10	24

The employed quantity of silica precursors did not have a significant influence on the hydrodynamic diameters of the SiNCs as the difference in the size of the six samples is only 36 nm and no unequivocal trend of an increase in size can be observed. Additionally, the PDIs are in a comparable range of around 0.10 as well, which is most likely caused by the fact, that the same emulsion was used for preparing the six samples with different silica concentrations. Both the mass of the precipitate and the solid content of the SiNCs dispersion seam to increase with increasing volume of used silica precursors, even though the trend is less steady for the mass of the formed precipitate. For all examined precursor concentrations, no significant reduction of the precipitate in perspective to the employed mass of silica precursors was achieved.

The TEM micrographs depicted in **Figure 21** emphasize, that the uniform capsules in the desired size range of about 300 nm are not obtained with low silica precursor concentrations. With only 15 µL of silica precursors, the formed shells are not continuous. The shells are fragmented and the obtained structures tend to aggregate. With 25 µL and 35 µL of silica precursors few nanocapsules with a high cavity-shell contrast are

observable, but the fraction of smaller structures in the size range below 100 nm, with no distinct shell outweighs.

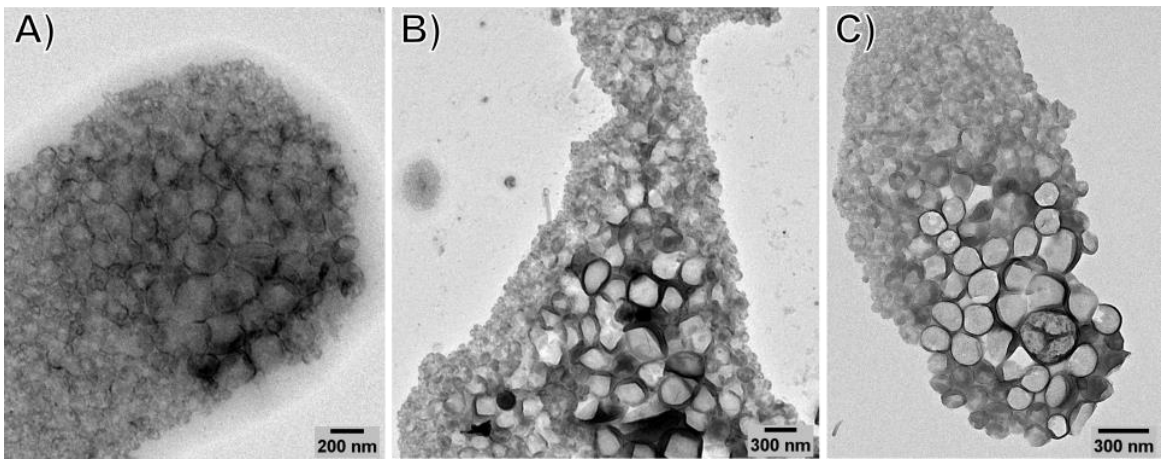

Figure 21: TEM micrographs of SiNCs synthesized with A) 15 µL (sample 1) B) 25 µL (sample 2) and C) 35 µL (sample 4) of silica precursor mixture.

The necessity to use at least 45 µL of silica precursors is also supported by the measured shell thickness of the capsules. When using 25 µL of silica precursor mixture, the average shell thickness is 6.5 ± 4.0 nm with about 58% of the shells being less than 6 nm thick. In comparison, the shell thickness increases to an average of 9.1 ± 3.2 nm when using 35 µL of the silica precursor mixture for synthesizing the capsules. As depicted in **Figure 22**, the majority of the shells for these capsules are in the size range of 6 – 10 nm. With an average shell thickness of 10.4 ± 2.5 nm, the capsules that were synthesized using 45 µL of the TMOS-APTES mixture exhibit the thickest shells. Moreover, the shell thickness becomes more consistent with an increasing amount of silica precursors used, as the deviation from the average is decreasing and more than 58% of the capsules have 8 – 12 nm thick capsule shells.

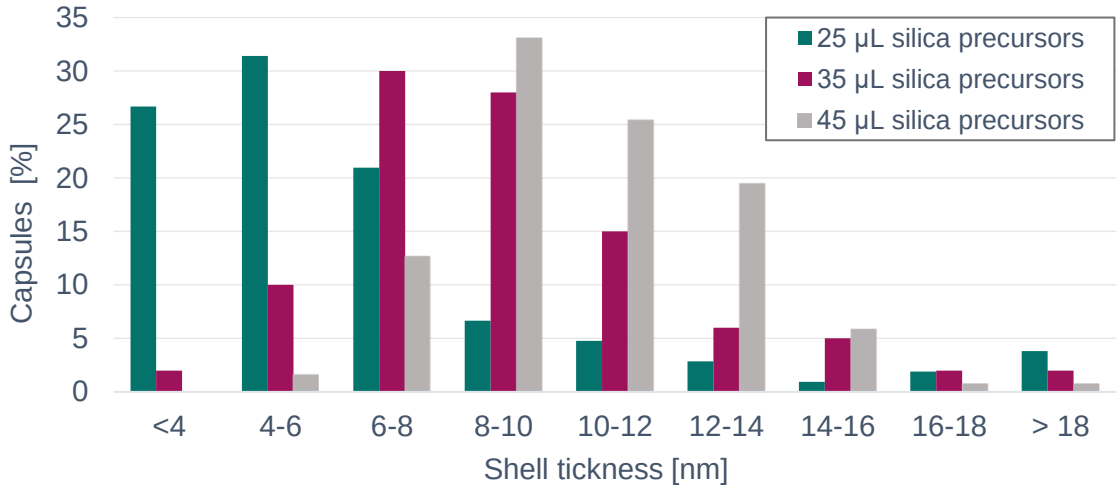

Figure 22: Shell thickness of SiNCs synthesized using 25 µL (green), 35 µL (red), or 45 µL (grey) of silica precursors. The thickness of the SiNCs was measured at at least 105 different points on the shells of various capsules for each capsule batch using the measuring tool in ImageJ.

In conclusion, the TEOS is not feasible as a replacement for TMOS in the synthesis of SiNCs without the addition of an additional external catalyst, as no uniform silica shell was formed. The shell thickness can be tuned by varying the amount of the employed silica precursors. In order to obtain capsules with a uniform shell and a homogenous size distribution, at least 45 µL of the 5.5:1 TMOS-APTES-precursor mixture should be added to 3 mL of emulsion.

4.1.4 Optimization of the surfactant

As the hydrolysis of TMOS and the following polycondensation has to take place at the interface of the aqueous droplets with the hydrophobic continuous phase, the surfactant was changed from PGPR to poly(ethylene-co-butylene)-*block*-poly(ethylene oxide) (PE/B-*b*-PEO) in an attempt to confine the hydrolysis at the interface and prevent precipitation.

The (PE/B-*b*-PEO) concentration was chosen according to the protocol from Li et al.[48], while the volumes of the continuous and the dispersed phase were identical to the capsule preparation with PGPR as the surfactant. Regarding the silica precursor addition, three different addition methods were tested. As depicted in **Figure 23**, mixtures of TMOS and APTES with two different amounts of cyclohexane and additional (PE/B-*b*-PEO) surfactant were added to the reaction mixtures A and C, while a TMOS-APTES mixture and a (PE/B-*b*-PEO) in cyclohexane solution were separately added to reaction mixture B.

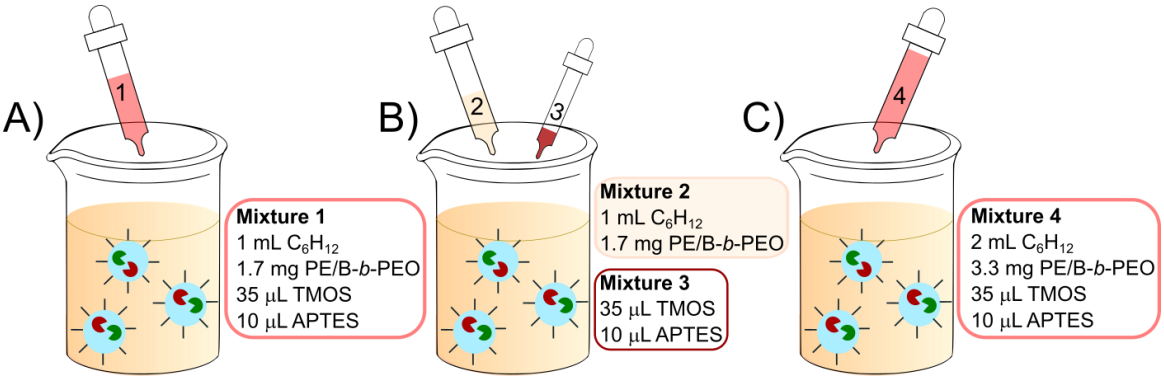

Figure 23: Schematic illustration of the addition of the different mixtures containing the silica precursors TMOS and APTES to the emulsions A-C.

After the reaction was finished, the formation of a white precipitate was observed for all three reaction mixtures with (PE/B-*b*-PEO) as the surfactant. As depicted in the photograph of the reaction mixtures after completion of the reaction in **Figure 24**, the formed solid is not precipitated completely. The supernatant was only slightly opaque and, in the case of sample C, it was even completely transparent. (PE/B-*b*-PEO) seems to stabilize the formed precipitate as well, since it is not settling down completely on the

bottom. This makes it more challenging to separate the desired SiNC-dispersion from the precipitate.

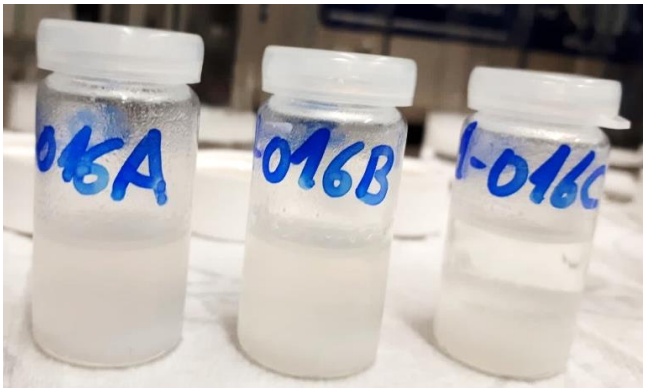

Figure 24: Photograph of the three different reaction mixtures A-C after completion of the reaction time.

The hydrodynamic diameters obtained from DLS measurements ranged from 368 nm to 490 nm, making the nanocapsules more than 20% larger, than the SiNCs fabricated with PGPR as the surfactant. The PDIs of the obtained capsules ranged from 0.15 to 0.27, which is comparable to the dispersity of the original SiNCs fabricated with PGPR. But the redispersion of the obtained SiNCs in water was not successful, as the measured PDIs increased drastically, and the hydrodynamic diameters measured in water did not correspond to the expected SiNC size (see **Table 8**).

Table 8: Hydrodynamic diameters and PDIs of the SiNCs of the samples A-C using (PE/B-*b*-PEO) as the surfactant. The measurements were made a) in cyclohexane and b) in water.

Sample	d_h[a] [nm]	PDI[a]	d_h[b] [nm]	PDI[b]
A	368	0.15	65	0.60
B	392	0.18	527	0.96
C	490	0.27	1071	0.31

Even though the TEM micrographs in **Figure 25** clearly display the formation of capsules in the desired size range of 250 – 350 nm, the transfer to aqueous medium was not successful, which might be caused by a less effective replacement of the (PE/B-*b*-PEO) surfactant with the high HLB surfactant Lutensol AT50. The TEM micrographs also show some structures, that show no contrast between the shell and the inner cavity, pointing to the formation of particles instead of capsules to some degree. Moreover, the capsules are surrounded by an unidentifiable structure and the size distribution of the capsules, that are visible on the TEM micrographs is broad with capsules ranging from less than 100 nm to more than 400 nm.

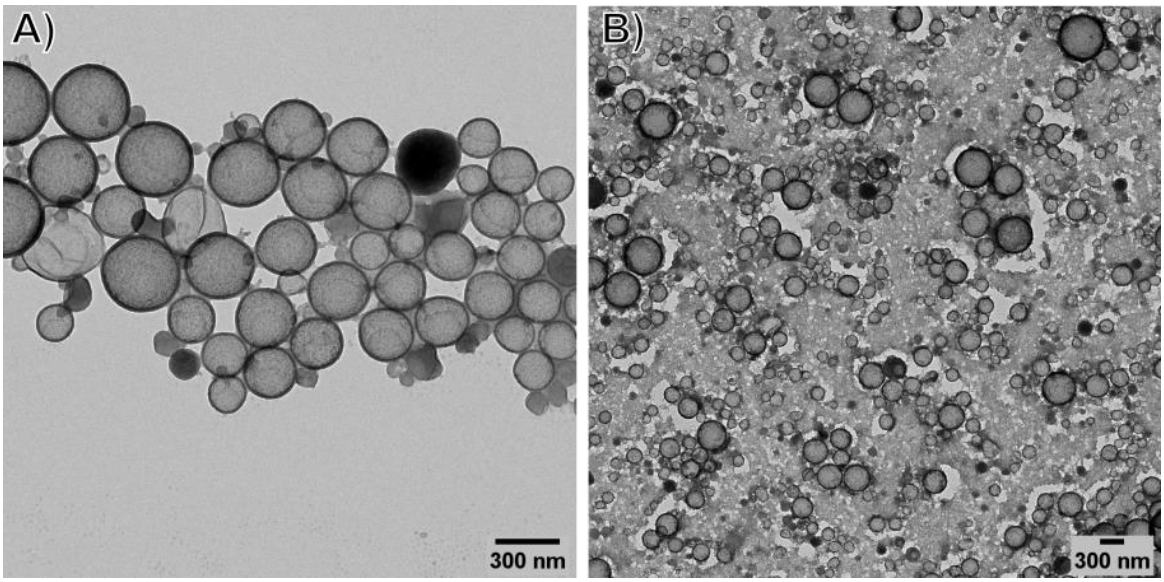

Figure 25: TEM micrographs of SiNCs synthesized from emulsion A with (PE/B-*b*-PEO) as the surfactant by adding mixture 1.

With an average shell thickness of 13.8 ± 4.8 nm, the SiNCs obtained from an emulsion with (PE/B-*b*-PEO) as the surfactant exhibit thicker shells than the capsules synthesized with PGPR. On the other hand, the higher deviation from the average shell thickness and the distribution of the respective shell thicknesses shown in **Figure 26**, stress that the formed shells show a high degree of irregularity.

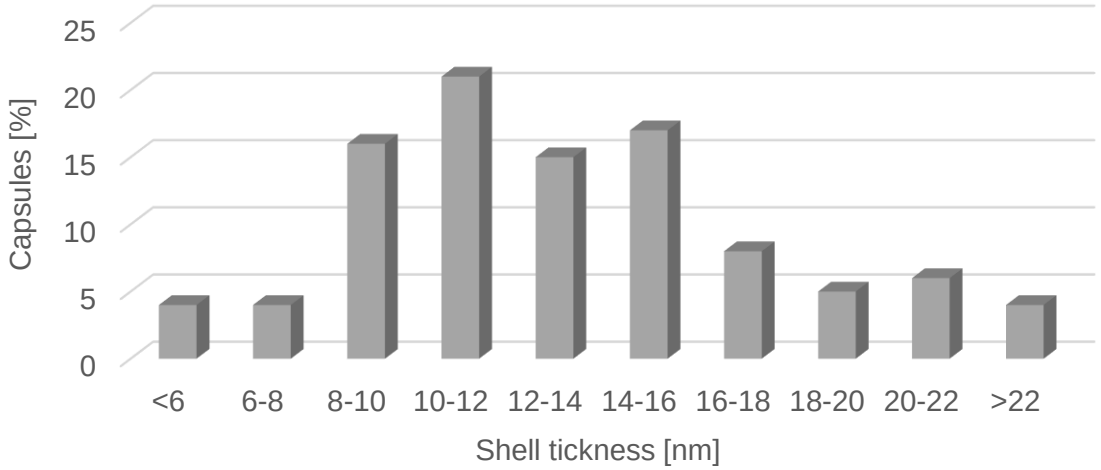

Figure 26: Shell thickness of SiNCs obtained with (PE/B-*b*-PEO) as the low-HLB surfactant. The thickness of the SiNCs was measured at 100 different points on the shells of various capsules using the measuring tool in ImageJ.

Overall, the formation of the precipitate during the SiNCs synthesis could not be prevented. Therefore, a centrifugation step was introduced in order to completely remove the precipitate before transferring the SiNCs to aqueous medium and PGPR was continuously employed as the low HLB surfactant.

When collectively summarizing the results of the downscaling of the synthesis of SiNCs for the fabrication of enzyme nanoreactors in cyclohexane, the following aspects are the most impactful: High-pressure homogenization was established as the preferable method for emulsion processing over ultrasonication, due to the better shell formation and high-pressure homogenization being gentler. Regarding the silica precursors, it was established that TEOS was not suitable for synthesizing the silica shells without the addition of any additional catalyst. Therefore, the most reactive alkoxide of silicone, TMOS has to be used or a different synthesis strategy with for example fluoride as the catalyst has to be chosen. Premixing TMOS and APTES before adding them to the emulsion was determined to be the preferable addition method. A clear trend was observed for the thickness of the shells, which increased with the amount of silica precursors (TMOS and APTES) used, with the highest thickness observed being 10.4 ± 2.5 nm. Lastly, PGPR was manifested as the surfactant of choice.

4.2 Optimizing the transfer of the SiNCs to aqueous medium

The established method for redispersing SiNCs in water is to add the dispersion of the SiNCs in cyclohexane dropwise to a solution of the high HLB surfactant Lutensol AT50 in water while shaking the solution by hand in the sonication bath to prevent the aggregation of the capsules. One of the major drawbacks of this technique is the inability to ensure reproducibility, as the manual shaking varies from batch to batch. When employing this technique for redispersing the SiNCs, aggregation of the SiNCs was observed in the majority of the samples as the obtained hydrodynamic diameters and PDIs were strikingly higher than the expected 250 – 350 nm and 0.1 – 0.3.

To overcome the challenges of the manual shaking and the manual addition, establishing an automatic process for the redispersion was attempted. Due to the lack of a device that was capable of shaking samples while they are in the sonication bath, an apparatus was constructed to achieve continuous shaking with an adjustable shaking intensity. To construct the shaking device the exchangeable blocks were removed from an MRK 23 thermomixer from Hettich and a cross clamp was attached to the metal pin previously used to fix the blocks. A metal rod construction was then fixed in the cross clamp and a tripod clamp for holding the sample was attached to its end. The thermomixer was then raised onto a platform so that the tripod clamp hung at a suitable height above the water level in the ultrasonic bath. A schematic of the obtained construction is depicted in **Figure 27**.

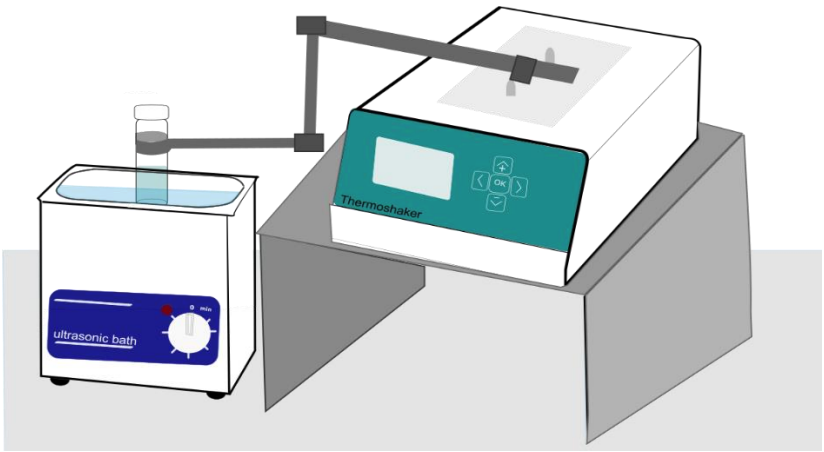

Figure 27: Schematic setup for using a thermomixer to redisperse the SiNCs in water. Dark grey rectangles symbolize the locations for attaching the cross clamps.

In contrast to the manual shaking the use of the automated shaking offered precise control over the shaking speed and as a starting point, 800 rpm were used for the transfer of the SiNCs to aqueous medium. During the optimization of the capsule synthesis in cyclohexane, the transfer to water was oftentimes insufficient, as a significant increase in capsule size and PDI could be observed. A direct comparison of the manual and the automatic shaking technique was made, by transferring two batches of GOx@SiNCs containing a high and a low GOx concentration to water using both techniques. A direct

comparison of the obtained DLS graphs including the respective hydrodynamic diameters and polydispersity indices is made in **Figure 28** for the high GOx concentration and in **Figure 29** for the low GOx concentration.

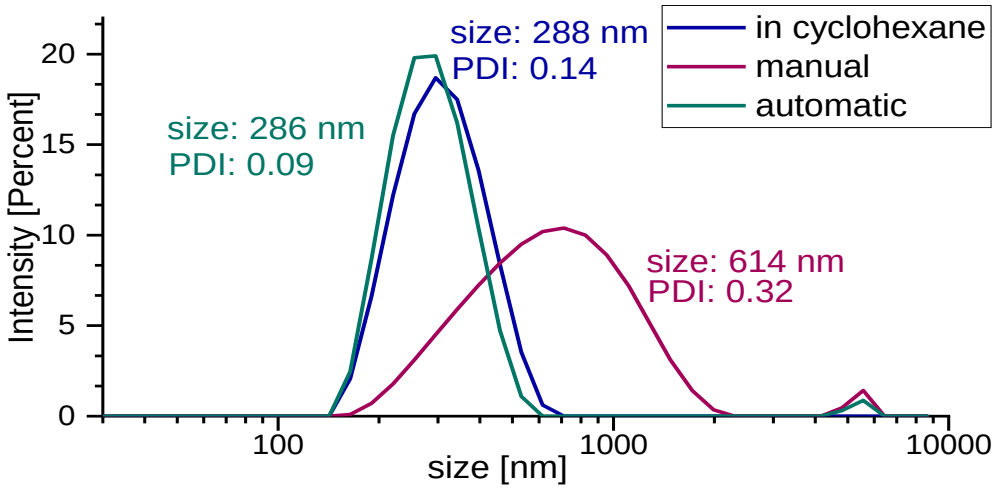

Figure 28: DLS graphs of the three measurements of GOx@SiNCs with a GOx concentration of 10 mg/mL in the dispersed phase after transferal to water using either automatic (green) or manual (pink) shaking. The average size and PDI are given in the corresponding colors.

The GOx@SiNCs with the higher GOx concentration had a diameter of 267 nm in cyclohexane with a PDI of 0.18, while the nanocapsules with the lower GOx concentration were slightly larger with a diameter of 306 ± 12 nm and a PDI of 0.19. Therefore, the two batches of manually redispersed capsules exhibited a high increase in both size and PDI. In comparison, the GOx@SiNCs redispersed using automatic shaking did not show a notable change in either size or PDI.

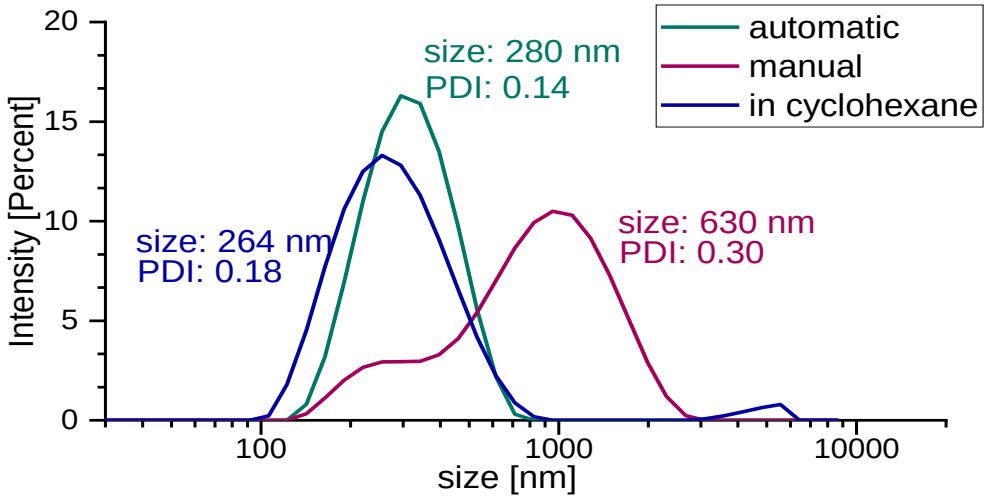

Figure 29*:* DLS graphs of the three measurements of GOx@SiNCs with a GOx concentration of 1 mg/mL in the dispersed phase after transferal to water using either automatic (green) or manual (pink) shaking. The average size and PDI are given in the corresponding colors.

As the redispersion with automatic shaking was successful for the synthesis of the GOx@SiNCs, it was employed for the redispersion of the GOx@SiNCs and HRP@SiNCs containing different enzyme concentrations that will be discussed in the upcoming section.

4.3 Synthesis of SiNCs with different GOx and HRP concentrations

Using the optimized down-scaled procedure for the synthesis of enzyme-loaded SiNCs in small volumes, SiNCs containing different concentrations of either GOx or HRP were successfully synthesized.

In order to check if GOx or HRP are aggregating when employing high concentrations of the respective enzymes, multiangle DLS measurements of both enzymes at various enzyme concentrations were carried out. As depicted in **Figure 30** small structures with a radius below 10 nm were detected at larger angles for HRP and at all angles for GOx. These peaks are likely to correspond to the non-aggregated GOx, which has dimensions of 7.7×6.0×5.2 nm^3 [49] and the non-aggregated HRP with dimensions of 6.2×4.3×1.2 nm^3.[50] On the other hand, the formation of aggregates in the µm-size range was observed for both GOx and HRP. Even though the distribution function exhibits higher intensities for these large aggregates, these aggregates make up only a small fraction of the entire sample because the scattering intensity is proportional to R^6. It was calculated that the fraction of aggregates is less than one part per million in comparison to the monomeric enzyme. Moreover, these aggregates were detected at all measured concentrations (4 to 32 mg/mL for GOx and 8 to 64 mg/mL for HRP) as shown in the appendix in **Figure 37** to **Figure 39**. Therefore, the aggregation of both GOx and HRP has no clear concentration dependence. As the aggregates were detected in all samples, they are not expected to have a significant decreasing effect on the enzyme activity at higher concentrations.

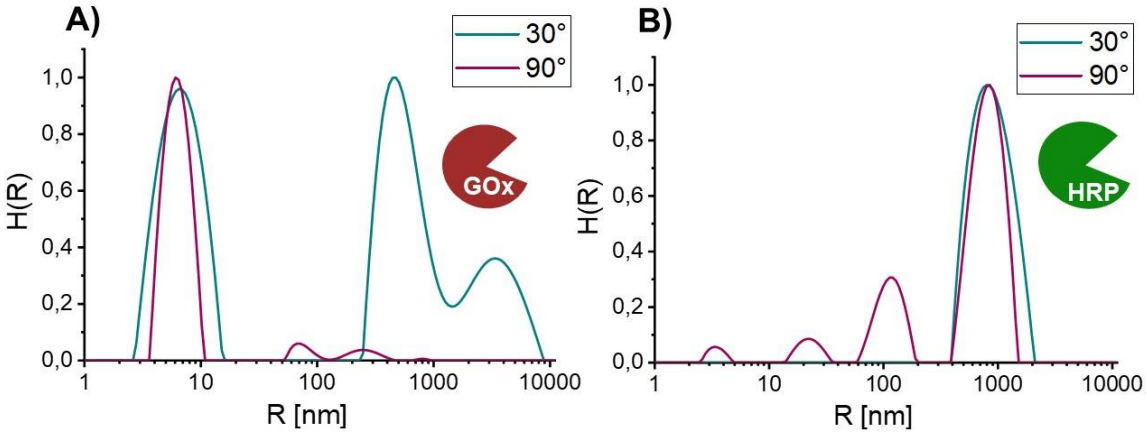

Figure 30: Distribution function H(R) of the radius R (intensity weighted) for A) 32 mg/mL glucose oxidase and B) 64 mg/mL HRP.

For the preparation of the GOx@SiNCs and the HRP@SiNCs, the chosen enzyme concentrations were 1 mg/mL, 5 mg/mL, and 10 mg/mL. For both enzymes, the sizes and PDIs of the emulsion droplets were nearly identical, independent of the used enzyme concentrations (see **Table 9** and **Table 10**).

Table 9: Hydrodynamic diameters and PDIs of the emulsion droplets used for fabricating GOx@SiNCs and the corresponding concentrations of GOx in the aqueous phase measured in cyclohexane.

Emulsion	*c*(Gox) [mg/mL]	*c*(Gox) [U/mL]	d_h [nm]	PDI
A	10	1452	218	0.15
B	5	726	205	0.13
C	1	145	208	0.15

Table 10: Hydrodynamic diameters and PDIs of the emulsion droplets used for fabricating HRP@SiNCs and the corresponding concentrations of HRP in the aqueous phase measured in cyclohexane.

Emulsion	*c*(HRP) [mg/mL]	*c*(HRP) [U/mL]	d_h [nm]	PDI
A	10	880	212	0.19
B	5	440	210	0.16
C	1	88	202	0.13

Each of the six emulsions was used to synthesize three independent batches of SiNCs to ensure the reproducibility of the results. The results of the DLS measurements are listed in **Table 11** for the GOx@SiNCs and in **Table 12** for the HRP@SiNCs. For the GOx@SiNCs the average diameter increased from 268 nm and 270 nm for the SiNCs with high and medium GOX concentrations to 302 nm for the SiNCs with the lowest GOx concentration. A similar trend was observed for the diameters of the HRP@SiNCs, whose diameters increase from 245 nm to 270 nm to 299 nm from the highest to the lowest HRP concentration. Overall, the size of all capsules shows a satisfactory reproducibility with only the HRP@SiNCs with 5 mg/mL of HRP showing a high variance in capsule diameter from batch to batch. For all 17 batches of SiNCs synthesized with encapsulated enzyme, the PDIs were below 0.25, speaking for a consistent, narrow size distribution and thus showing the success of the developed SiNCs synthesis for small volumes. Moreover, TEM micrographs (see **Figure 40** and **Figure 41** in the appendix) were measured for the capsules with the highest and the lowest enzyme concentration for both HRP and GOx. The thicknesses of the shells were estimated as 10.2 ± 2.8 nm for the GOx@SiNCs with the high and 10.5 ± 4.2 nm for the GOx@SiNCs with the low GOx concentration. With HRP

the capsules with the high concentrations had 15.1 ± 4.9 nm and the HRP@SiNCs with the lowest HRP concentration encapsulated had 12.4 ± 3.2 nm thick shells on average.

Table 11: Hydrodynamic diameters and PDIs of the three batches of GOx@SiNCs synthesized from each emulsion measured in cyclohexane.

***c*(Gox)**	**10 [mg/mL]**		**5 [mg/mL]**		**1 [mg/mL]**	
Sample	**d_h [nm]**	**PDI**	**d_h [nm]**	**PDI**	**d_h [nm]**	**PDI**
1	274	0.20	280	0.23	289	0.18
2	262	0.17	271	0.21	311	0.19
3	267	0.18	259	0.19	306	0.19

Table 12: Hydrodynamic diameters and PDIs of the three batches of HRP@SiNCs synthesized from each emulsion measured in cyclohexane.

***c*(HRP)**	**10 [mg/mL]**		**5 [mg/mL]**		**1 [mg/mL]**	
Sample	**d_h [nm]**	**PDI**	**d_h [nm]**	**PDI**	**d_h [nm]**	**PDI**
1	249	0.15	328	0.09	302	0.14
2	241	0.15	274	0.16	295	0.13
3	-	-	209	0.21	300	0.12

The obtained SiNCs were all successfully transferred to aqueous medium using the automatic shaking method described in the previous section. The hydrodynamic diameters and the PDIs of the GOx@SiNCs and HRP@SiNCs are listed in **Table 13**. Overall, the sizes in water are close to the capsule sizes in cyclohexane, with two batches showing an increase in size to more than 400 nm, which can be caused by either swelling of the nanocapsules in water or the formation of small aggregates. The measured PDIs suggest a narrow size distribution of the capsules in water. Nonetheless, it cannot be verified, that the capsules are not destroyed during redispersion, even though the DLS-measurements suggest otherwise.

Table 13: Hydrodynamic diameters, PDIs and solid contents (SC) of the HRP@SiNCs and GOx@SiNCs after the transfer to water.

***c* [mg/mL]**	**HRP@SiNCs**			**GOx@SiNCs**		
	d_h [nm]	**PDI**	**SC [mg/mL]**	**d_h [nm]**	**PDI**	**SC [mg/mL]**
10	260	0.18	6.42	279	0.16	5.10
5	308	0.14	5.90	485	0.22	5.31
1	423	0.22	5.42	280	0.14	5.16

4.4 Quantification of enzymes encapsulated in the nanocapsules

To prove that the enzyme that was dissolved in the aqueous phase before forming the SiNCs was successfully encapsulated, the encapsulation efficiency has to be determined. Moreover, the actual enzyme concentration inside of the SiNCs has to be verified in order to be able to compare the catalytic activity of the nanocapsules with different enzyme concentrations. To do so, the capsules have to be separated from the non-encapsulated enzyme in the dispersion, which can be achieved via centrifugation. Usually, several centrifugation runs are performed and the enzyme concentrations in all the collected pellets and the final supernatant can be measured afterwards in order to calculate the encapsulation efficiency.

A Micro-BCA (bicinchoninic acid) protein assay was chosen to determine the protein concentration. The assay has a linear working range of 2 – 40 µg/mL, which is in conformity with the calculated enzyme concentrations for 100% encapsulation efficiency that are expected to range from 3.9 µg/mL for the lowest to 38.9 µg/mL for the highest deployed enzyme concentration. The BCA-assay is a colorimetric method for the quantification of the total protein amount, based on the biuret reaction of the protein with Cu^{2+}. As depicted in **Figure 31** the resulting Cu^{+}-ions are forming a complex of intense purple colour with the bicinchoninic acid molecules. By measuring the absorbance, the coloured complex can be used to monitor the amount of cuprous ions produced and hence calculate the protein concentration.[51]

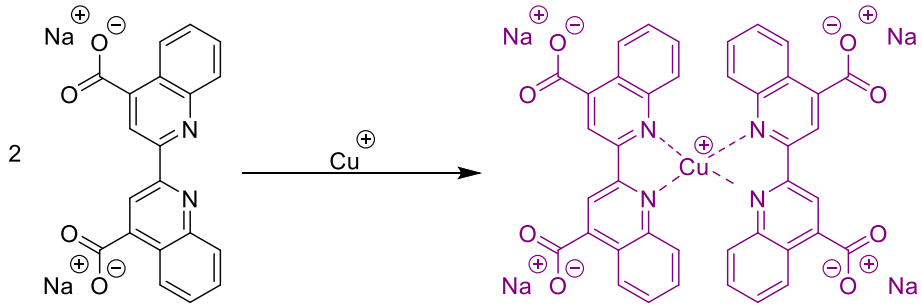

Figure 31: Reaction of two molecules of BCA with one Cu^{+}-ion that was formed by reduction of a Cu^{2+}-ion in a peptide-mediated biuret reaction.

In order to calculate the samples' protein concentration a calibration curve with different concentrations of a protein standard has to be used. Usually, Bovine serum albumin (BSA) is used as the protein standard, but as the accuracy of the calculated protein concentration depends on the used standard, another calibration curve with GOx was prepared. Three samples with known GOx concentrations were prepared and their concentrations were then calculated using the BSA and the GOx calibration curve (see **Figure 42**, in the appendix). As shown by the result in **Table 14**, some deviation from the known concentration was observed with both calibration curves. Nonetheless, the use of GOx for

calibration was more accurate and therefore GOx was used as the calibration substance for all further measurements.

Table 14: Known concentration of glucose oxidase in comparison to the concentrations determined with the BCA-assay using either bovine serum albumin or glucose oxidase for calibration.

$c(GOx)_{prepared}$ [µg/mL]	$c(GOx)_{BSA}$ [µg/mL]	$c(GOx)_{GOx}$ [µg/mL]
25	17.3	25.9
50	31.1	47.1
100	50.4	81.6

As silica absorbs at 562 nm, which is that is used to record the BCA-copper-complex, empty SiNCs have to be used as a control sample, when determining the encapsulation efficiency with the BCA-assay. However, when adding BCA-working reagent to the empty SiNCs, a change from green to purple was observed within a few minutes. Moreover, the recorded absorbance of the control sample is with an absorbance of 1.47 ± 0.02 a lot higher than the added absorptions of the separately measured SiNCs with 0.67 ± 0.4 and the BCA working reagent with 0.120 ± 0.002. As contamination of the buffer and the BCA reagent could be excluded, it must be assumed that the empty SiNCs are also able to reduce the copper and thus induce the color change caused by the complexation of Cu^{+}. As the empty SiNCs are not applicable as a control sample, the BCA-assay is not suitable for determining the encapsulation efficiency and the absolute enzyme concentration within the capsules. As the absolute enzyme concentration is required to compare the catalytic activities of the enzyme nonreactors with different concentrations of encapsulated enzyme, the activity assays could not be performed up to now. Besides the BCA-Assay, several other well-established protein assays, that are not based on the chelation of copper, exist and could be tested for determining the encapsulation efficiency as for example the dye-based Coomassie blue assay. Unfortunately, many protein assays are not compatible with samples containing surfactants and are highly dependent on the sample´s protein concentration and the type of protein to be quantified. This makes a detailed assessment of the compatibility of the accessible protein assays with the enzyme-containing SiNCs necessary, before testing a different protein assay.[52]

An alternative more versatile method, that is commonly used to determine the encapsulation efficiency is thermogravimetric analysis (TGA). With this method, a sample of empty nanocapsules is subjected to a heating rate whilst recording the weight loss of the SiNCs over time. The enzyme-containing nanocapsules are measured in the same way and any further weight losses in comparison to the empty capsules are attributed to the presence of the enzymes. As this method was already applied to determine the

encapsulation of several different enzymes,[2] it is the method of choice for future experiments.

4.5 Synthesis of fluorescently labeled SiNCs for cell uptake experiments

In order to conduct cell uptake experiments with the GOx@SiNCs, the capsules need to be detectable. For this purpose, the capsules were fluorescently labelled with Cyanine 5 (Cy5) – a dye with an emission maximum at 662 nm. For labelling, the NHS-ester of Cy5 was reacted with the APTES silica precursor before synthesizing the SiNCs. The reaction of the primary amine of APTES with the Cy5-NHS-ester yields a silica precursor that is linked to the fluorophore via stable amide bonds as shown in **Figure 32.**

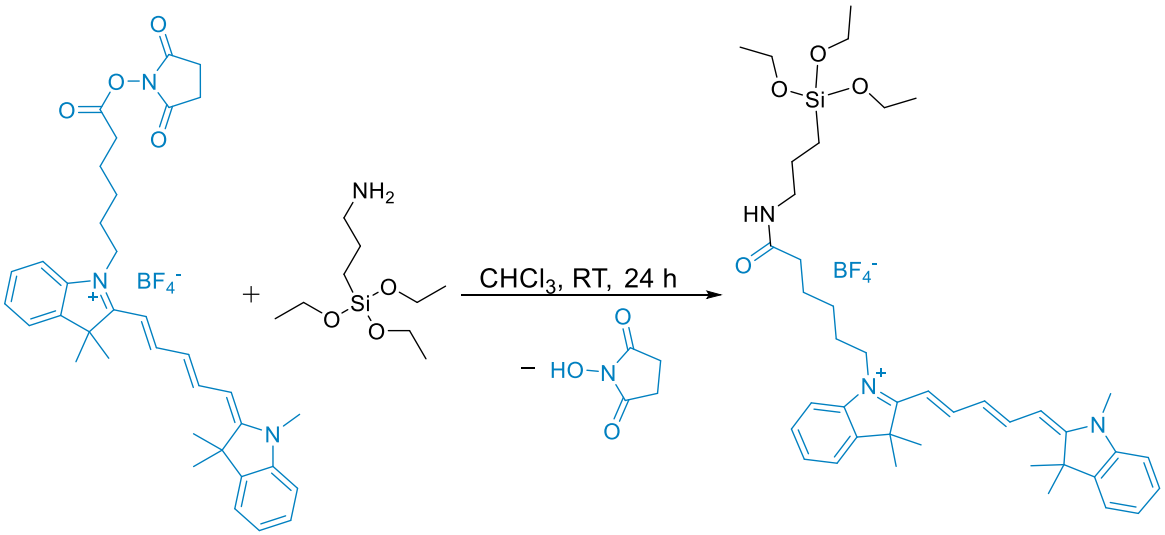

Figure 32: Schematic of the reaction of Cy5-NHS-ester with APTES forming the fluorescent silica precursor Cy5-APTES.

The Cy5-APTES is then added to the regularly used APTES and TMOS precursors when synthesizing GOx@SiNCs. The hydrodynamic diameters and PDIs of the emulsion and the capsules in both cyclohexane and water are listed in

Table 15.

Table 15: Hydrodynamic diameter and PDI of the emulsion droplets and SiNCs measured in a) cyclohexane or b) water.

Emulsion		SiNCs			
d_h[a] [nm]	PDI[a]	d_h[a] [nm]	PDI[a]	d_h[b] [nm]	PDI[b]
273	0.19	331	0.23	329	0.24

As the size and the dispersity of the fluorescently labelled capsules are comparable to those of the unlabeled SiNCs and the fluorescence was checked to be sufficient, the capsules were used to conduct the cell uptake experiment described in the following section.

4.6 Cell uptake of GOx@SiNCs by HCT 116 cells

One possible field of application for the silica nanoreactors with encapsulated enzymes are therapeutics because many enzymes cannot be administered directly, as they show insufficient cellular uptake and are unstable in biological media. The increased stability and protection offered by the encapsulation in the SiNCs can improve the bioavailability of the enzymes, if the SiNCs exhibit a sufficient cell uptake.[40] As GOx containing SiNCs could be employed to produce hydrogen peroxide intracellularly to function as oncolytic nanoreactors, HCT 116 cells, a human colorectal carcinoma cell line was used to study the cell uptake via flow cytometry.

As depicted in the graph in **Figure 33**, the median fluorescence intensity is increasing with longer incubation times reaching its maximum 8 h after uptake. The high fluorescence after 4 h indicates a rapid uptake of high quantities of the SiNCs. For the longer incubation times, immense cell toxicity is indicated by the error bars and was also observable by eye.

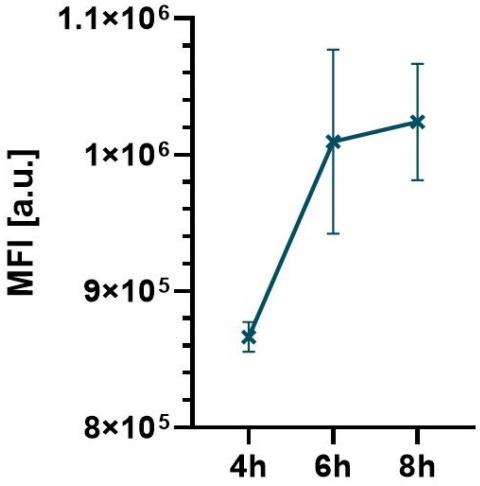

Figure 33: Median fluorescence intensities (MFIs) measured after the different incubation times.

Overall, the flow cytometry measurement show, that the GOx@SiNCs exhibit a rapid uptake by the HCT 116 cells. The high cell toxicity can be caused by either the SiNCs themselves or by the production of H_2O_2 by the GOx@SiNCs, as the used cell culture medium contains a high concentration of glucose. In order to study the cause of the high cell toxicity, cell toxicity experiments have to be conducted comparing empty SiNCs to GOx@SiNCs and HRP@SiNCs.

5. Conclusions and Outlook

The aim of this thesis was to develop a synthesis strategy for enzyme-loaded SiNCs in small quantities to enable the comparison of different enzyme concentrations while reducing the required overall amount of enzyme. The procedure for synthesizing large volumes of SiNCs described by Jiang et al.[5] was used as the starting point for the optimization. With this method, the SiNCs were prepared in an inverse (water-in-oil) miniemulsion, with the enzymes dissolved in the dispersed phase to directly encapsulate them during the shell formation and transferring the SiNCs to aqueous medium afterwards.

In the course of the optimization, high-pressure homogenization was established as the superior emulsification technique in comparison to ultrasonication, because uniform and continuous silica shells were only formed when using high-pressure homogenization. Moreover, high-pressure homogenization is a gentler emulsification technique and the high stress and increasing temperature during ultrasonication could affect the enzyme activity. When interchanging TMOS with TEOS, the synthesis of SiNCs was not successful, as the formed shells were very thin and fragmented. Therefore, TMOS appears to be the only silicon alkoxide, that does not require the addition of an external catalyst to form continuous shells, as it is the most reactive of the silicon alkoxides. Even though the same ratio of TMOS to APTES was used for all synthesis, the variation of the total precursor amount showed, that the thickness of the obtained silica shells increases with an increasing amount of silica precursors added. The highest tested amount of silica precursors led to a shell thickness of 10.4 ± 2.5 nm. Additionally, premixing TMOS and APTES before adding them to the emulsion was determined to be the most reliable method for the silica precursor addition. (PE/B-*b*-PEO) was tested as an alternative low HLB surfactant to PGPR, but the SiNCs fabricated with (PE/B-*b*-PEO) as the surfactant exhibited larger diameters, more irregular shell thicknesses and were more challenging to separate from the formed precipitate. Hence, PGPR was manifested to be the preferable choice for the low HLB surfactant. As the formation of the precipitate could not be prevented, a centrifugation step to remove the precipitate before transferring the capsules to aqueous medium was introduced in the course of the synthesis optimization. With these optimized conditions for the synthesis of enzyme encapsulating SiNCs in small quantities, GOx@SiNCs and HRP@SiNCs with three different concentrations of each enzyme were successfully synthesized.

For transferring the SiNCs to aqueous medium, a new technique employing automatic shaking instead of manual shaking in the sonication bath was introduced. The automatic shaking provides the means to improve the redispersion process by offering precisely controllable shaking speeds leading to better reproducibility.

The encapsulation efficiency was supposed to be determined using a BCA-assay, but since the control sample of empty SiNCs reacted with the BCA reaction mixture, quantifying the concentration of the encapsulated enzymes was not possible. Nonetheless, fluorescently labelled GOx@SiNCs were synthesized and a rapid uptake of these capsules by HCT 116 cells was observed via flow cytometry.

As depicted in **Figure 34**, the structural properties of the SiNCs are directly influenced by the chosen synthesis parameters. Additionally, the enzymatic activities of the nanoreactors, the cell uptake and the cytotoxicity depend on the capsule morphology and therefore also on the chosen synthetic conditions, making the optimization of the enzymatic activity a complex task.

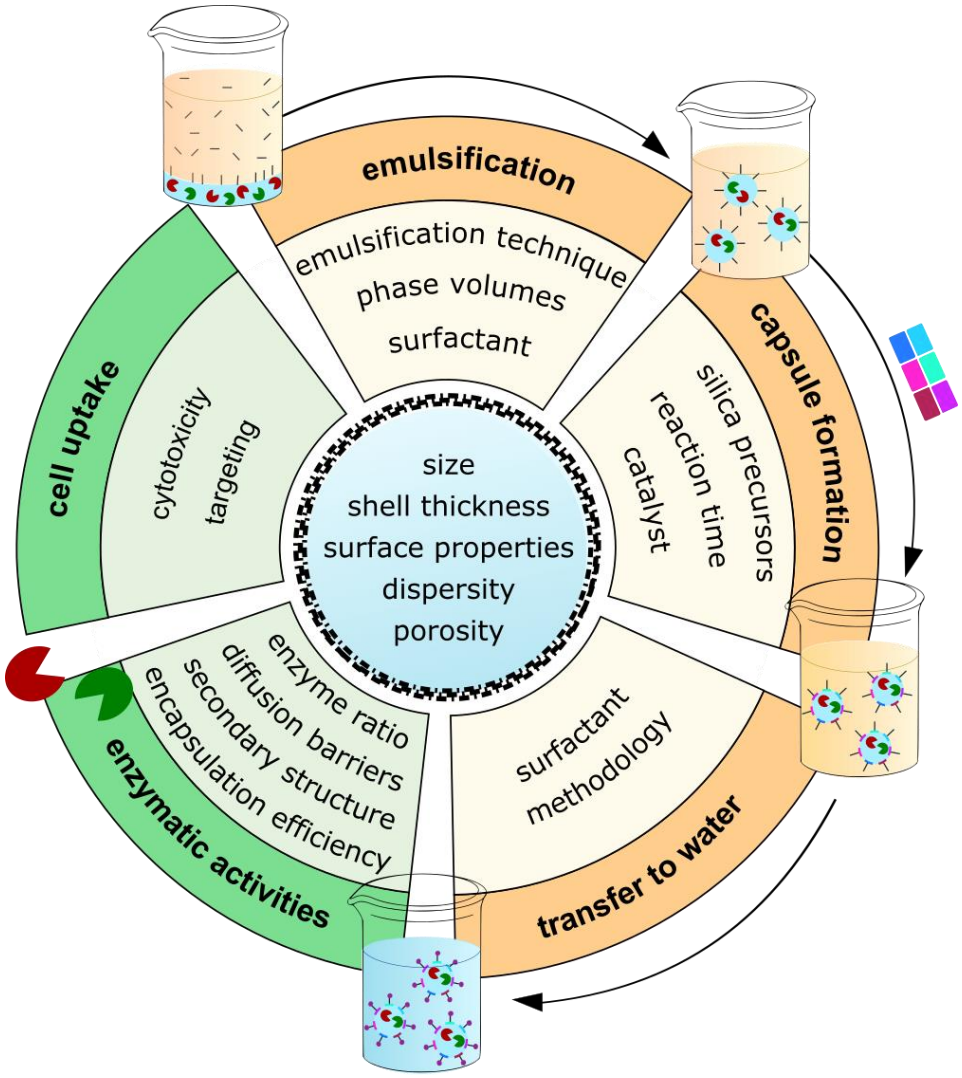

Figure 34: Synthetic parameters (yellow) and application related properties (green) that have to be monitored and have a direct impact or are directly impacted by the structural properties of SiNCs (blue).

In order to solve this complex problem, the following aspects have to be addressed in the future: At first, several batches of empty SiNCs should be synthesized to collect a sufficient

amount of precipitate for characterization e.g. via solid-state NMR. Determining the composition of the precipitate could help to develop new strategies for preventing the precipitate formation. Such strategies could include testing different amine-containing silica precursors as alternatives to APTES or choosing a different synthetic strategy with TEOS and fluoride as an additional external catalyst.

To gain a better understanding of the interfacial sol-gel process forming the silica shells, pH-sensitive dyes could be employed to monitor the local pH at the interface and verify the assumed occurrence of a base catalyzed sol-gel reaction at the interface. Moreover, testing higher amounts of silica precursors has to be considered to achieve thicker shells comparable to the 30 nm thick shells of the TEOS/APTMS-SiNCs obtained by a fluoride catalyzed sol-gel reaction.[2]

As the automatic shaking was introduced as a new technique, systematic testing of the chosen parameters needs to be done. For this purpose, several batches of SiNCs that are comparable in size in cyclohexane must be synthesized and then transferred to aqueous medium using different conditions. The parameters that can be varied are the shaking speed (200 to 1200 rpm), the shaking time, the volume ratio of SiNC-dispersion to aqueous medium, the surfactant concentration and the stirring speed after redispersion. Moreover, this technique cannot only be used for the transfer of SiNCs to aqueous medium but it can be used for other nanoparticles and nanocapsules synthesized in an inverse emulsion as well.

For optimizing the amount of both GOx and HRP encapsulated in the SiNCs, samples of the SiNCS containing the same overall enzyme concentration have to be prepared, even though the concentration of enzymes inside the nanocapsules varies. To do so, the encapsulation efficiency has to be measured to determine the enzyme concentration inside the capsules. As the BCA-assay was found to be incompatible with the SiNCs, thermogravimetric analysis could be used as an alternative method for determining the encapsulation efficiency. Afterwards, the enzymatic activity of the different GOx@SiNCs and the HRP@SiNCs will have to be analyzed using the Amplex Red assay. As depicted in **Figure 35** Amplex Red (10-acetyl-3,7-dihydroxyphenoxazine) is a colorless substrate for peroxidase and since glucose oxidase and peroxidase mediated reactions can be coupled, it can be used to examine the activity of both enzymes.[53]

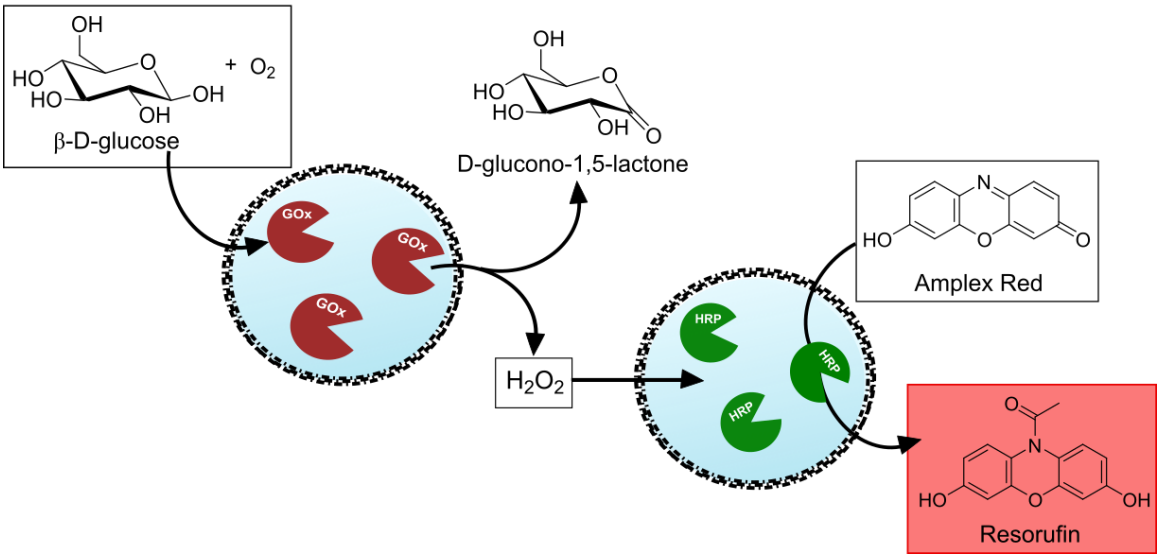

Figure 35: Amplex Red Assay for evaluating the enzymatic activity of GOx and HRP encapsulated in SiNCs

In this assay, glucose oxidase reacts with D-glucose to form D-gluconolactone and H_2O_2, which is a substrate for HRP. The H_2O_2 reacts in a 1:1 ratio with Amplex Red in the presence of HRP, forming the red-fluorescent resorufin. The generated fluorescence is monitored to assess the enzyme activity. To study the activity of just GOx@SiNCs, non-encapsulated HRP is used instead of HRP@SiNCs and to examine the activity of HRP in the SiNCs H_2O_2 can be used directly as the substrate. The Michaelis-Menten-kinetics can be obtained by altering the substrate concentrations for each enzyme which is glucose for GOx and H_2O_2 for HRP. In conclusion, optimizing the amount of enzyme encapsulated within the SiNCs requires the encapsulation of more than three different concentrations of each enzyme and the subsequent characterization and assessment of the enzyme activity using the Amplex Red Assay.

From a long-term perspective, the enzyme-loaded SiNCs should also be tested for their usability as synthetic organelles in both artificial and living cells. For this purpose, the uptake of the SiNCs, their cytotoxicity and the enzyme activity inside of living cells have to be studied.

6. Experimental Procedures

6.1 Materials

All solvents and reagents were obtained from commercial suppliers and used as received unless stated otherwise. Cyclohexane (≥99.5%) was obtained from VWR Chemicals and stored over molecular sieve. Polyglycerol polyricinoleate (GRINDSTED®PGPR 90) was kindly gifted from Danisco and Lutensol AT50 powder was supplied by BASF. Tetramethyl orthosilicate (TMOS, 98%), (3-Aminopropyl)triethoxysilane (APTES, 99%) and Dulbecco´s Phosphate buffered saline (pH 7.1 – 7.5, 1x) were purchased from Sigma-Aldrich. The amine-reactive fluorescent dye Cyanine5 NHS ester (Cy5-NHS) was purchased from Lumiprobe GmbH, Germany. The surfactant poly((ethylene-co-butylene)-block-(ethylene oxide)), P((E/B)-b-EO), consisting of a poly(ethylene-co-butylene) block (NMR: M_n = 3700 g mol^{-1}) and a poly(ethylene oxide) block (NMR: M_n = 2900 g mol^{-1}) was synthesized according to a reported procedure by Schlaad et al.[54]

The employed enzymes glucose oxidase from *Aspergillus niger* (GOx, Type X-S, lyophilized powder, 100,000-250,000 units/g solid, G7141-50KU) and peroxidase from horseradish (HRP, Type I, essentially salt-free, lyophilized powder, 50-150 units/mg solid, P8125-100KU) were supplied by Sigma-Aldrich as well. Dulbecco's Modified Eagle's Medium (DMEM) with high glucose and 0.25% Trypsin-EDTA solution were obtained from Gibco™ and the Zombie aqua™ fixable viability kit from BioLegend, USA.

6.2 Methods of Characterization

Dynamic Light Scattering (DLS)

For determining the size of the nanocapsules dynamic light scattering (DLS) measurements were conducted at an angle of 90° with a Malvern Zetasizer Nano-S90. For measurements in cyclohexane, 50 µL of SiNC dispersion or emulsion were diluted with 500 µL of cyclohexane while for measurements in water 100 µL of aqueous SiNCs dispersion were diluted with 500 µL of milli-Q water.

Multi-Angle Dynamic Light Scattering (MADLS)

Light scattering measurements at different angles were performed on an ALV spectrometer with a He-Ne laser (wavelength of 632.8 nm) as the light source. The spectrometer is equipped with a goniometer and an ALV-5004 multiple-tau full-digital correlator (320 channels), allowing measurements over an angular range from 30° to 150°. For temperature-controlled measurements, the light scattering instrument is equipped with a thermostat from Julabo. The measurements were performed at 20 °C at nine different angles ranging from 30° to 150° and the ALV5000 software was used for data processing.

Transmission electron microscopy (TEM)

A JEOL1400 microscope was used for transmission electron microscopy (TEM) and an acceleration voltage of 120 kV was used. The samples were deposited on carbon-coated copper grids. The analysis of particle sizes was done with ImageJ.

6.3 Optimization of the SiNC synthesis in small volumes

6.3.1 Synthesis of SiNCs with different emulsification methods

An inverse (water-in-oil) miniemulsion was employed to synthesize the SiNCs. For each of the two studied emulsification methods, two emulsions were prepared separately. The continuous phase of each sample consisted of 10 mL of a premade solution of PGPR (26.7 mg/mL) in cyclohexane. For the emulsion preparation, the continuous phase was added to the aqueous phase, consisting of 350 µL of Dulbeccos´s phosphate-buffered saline (DPBS) under magnetic stirring at 750 rpm. Afterwards, the four mixtures were homogenized with a T18 Ultra-Turrax at 13.000 rpm for 1 min. Two samples were then sonicated with a Branson 450W sonifier with a 1/2´ tip under ice cooling. A pulse mode with 20 s ultrasonication and 10 s pause was used for a total ultrasonication time of 180 s at 30% amplitude. The other two samples were processed with a low volume microfluidizer (LV1, microfluidics corporation) with a Y-shape interaction chamber with 75 µm channels at 8000 psi in two cycles. Afterwards, the obtained emulsions were divided into three samples of 3 mL each and a mixture of 35 µL TMOS and 10 µL APTES was added to each sample while stirring at 750 rpm at room temperature. After stirring the reaction mixtures for 4 h, the samples were centrifuged at 300 g for 3 min at 20 °C to remove the precipitate and then transferring the SiNCs to aqueous medium.

For the transfer to water 0.6 mL of the nanocapsule cyclohexane dispersion were added dropwise to 6 mL of aqueous Lutensol AT50 (0.3 wt%) solution under manual shaking in a sonication bath. After 5 min of shaking the solution was kept stirring at 750 rpm in an open vial for 24 h to remove the cyclohexane by evaporation.

6.3.2 Synthesis of SiNCs with different precursor addition

For testing the precursor addition, two emulsions were prepared using the same conditions as described above for the two samples using high-pressure homogenization for emulsification. After dividing the emulsions into samples of 3 mL each, the silica precursors were added in three different fashions. To the first sample, the 35 µL TMOS and 10 µL APTES were added separately, while a mixture of 35 µL TMOS and 10 µL APTES was added to the second sample. For the third sample, a mixture of 35 µL TMOS and 10 µL APTES in 1 mL of cyclohexane containing 13.3 mg PGPR was added while stirring at 750 rpm. All three reactions were stirred for 5 h at 750 rpm at room temperature.

6.3.3 Synthesis of SiNCs with TEOS

When using TEOS instead of TMOS for synthesizing the SiNCs, two emulsions were prepared using the LV1 microfluidizer under the same conditions described in subsection 6.3.1. A mixture of 52.5 µL of TEOS and 10 µL APTES were added to each sample of 3 mL while stirring at 750 rpm. All three reactions were stirred for 4 h at 750 rpm at room temperature.

6.3.4 Synthesis of SiNCs with different precursor amounts

Two emulsions, with 10 mL of a premade solution of PGPR (26.7 mg/mL [1]) in cyclohexane as the continuous phase and 350 µL of DPBS as the dispersed phase, were prepared separately. For the emulsion preparation, the continuous phase was added to the aqueous phase under magnetic stirring at 750 rpm followed by homogenization with a T18 Ultra-Turrax at 13.000 rpm for 1 min. Both samples were processed with a low volume microfluidizer (LV1, microfluidics corporation) with a Y-shape interaction chamber with 75 µm channels at 8000 psi in two cycles, before combining the samples into one emulsion. This collective emulsion was then divided into six samples of 3 mL each.
For testing different amounts of the silica precursors, while not altering the TMOS:APTES ratio, a mixture of 350 µL TMOS and 100 µL APTES was prepared. Different volumes of the silica precursor mixture (15, 25, 30, 35, 40 and 45 µL) were then added to each sample while stirring at 750 rpm. After 4 h of reaction time, the supernatant was removed and the amount of formed precipitate and the solid content in the supernatant was estimated.

6.3.5 Synthesis of SiNCs with (PE/B-*b*-PEO)

An inverse (water-in-oil) miniemulsion was prepared with the continuous phase consisting of 10 mL cyclohexane and 35.9 mg of(PE/B-*b*-PEO). The solution of (PE/B-*b*-PEO) in cyclohexane was sonicated at 40 °C in the sonication bath for 30 min, before adding it to the aqueous phase, consisting of 350 µL DPBS while stirring at 1000 rpm. Afterwards, the mixture was homogenized with a T18 Ultra-Turrax at 13.000 rpm for 1 min and processed with a low volume microfluidizer (LV1, microfluidics corporation) with a Y-shape interaction chamber with 75 µm channels at 8000 psi in two cycles. Afterwards, the obtained emulsion was divided into three samples of 3 mL. To each of the samples, the silica precursors were added in a different fashion. For the first sample, 1.67 mg of (PE/B-*b*-PEO) were dissolved in 1 mL cyclohexane at 40 °C in the sonication bath. After cooling to room temperature, 35 µL of TMOS and 10 µL of APTES were added to this solution which was then added dropwise to the previously made emulsion. For the second sample, 1.67 mg of were dissolved in 1 mL cyclohexane at 40 °C in the sonication bath. After cooling to room temperature this solution was added dropwise to the sample before adding a mixture of

35 µL of TMOS and 10 µL of APTES. Lastly, 3.33 mg of (PE/B-*b*-PEO) were dissolved in 2 mL cyclohexane at 40 °C in the sonication bath. After cooling to room temperature 35 µL of TMOS and 10 µL of APTES were added to this solution which was then added dropwise to the previously made emulsion. All three samples were stirred at 750 rpm at room temperature for a total of 5 h.

6.4 Synthesis of enzyme-loaded SiNCs

During the formation of the nanocapsules, the enzymes were directly encapsulated into the aqueous core by pre-dissolving the enzymes in Dulbecco's phosphate-buffered saline (350 µL) by thermoshaking at 500 rpm and 20 °C for 15 min. The employed enzyme concentrations and ratios are listed in **Table 16**.

Table 16: Employed concentrations of GOx and HRP in the aqueous phase employed for synthesizing the enzyme encapsulated SiNCs.

Sample	GOx@SiNCs		HRP@SiNCs	
	c [mg/mL]	*c* [U/mL]	*c* [mg/mL]	*c* [U/mL]
1	10	1452	10	880
2	5	726	5	440
3	1	145,2	1	88

The continuous phase consisted of 10 mL of a premade solution of PGPR (26.7 mg/mL) in cyclohexane. For the emulsion preparation, the continuous phase was added to the aqueous phase under magnetic stirring at 750 rpm and the mixture was homogenized with a T18 Ultra-Turrax at 13.000 rpm for 1 min. Then the emulsion was processed with a low volume microfluidizer (LV1, microfluidics corporation) with a Y-shape interaction chamber with 75 µm channels at 8000 psi in two cycles. After the emulsification, the emulsion was divided into three samples of 3 mL each and a mixture of 35 µL TMOS and 10 µL APTES were added to each sample while stirring at 750 rpm at room temperature. After stirring the reaction mixture for 4 h the precipitate was removed by centrifuging at 300 g for 3 min at 20 °C.

For transferring nanocapsules to aqueous medium, 0.6 mL of the nanocapsule cyclohexane dispersion were added dropwise to 6 mL of aqueous Lutensol AT50 (0.3 wt%) solution under automatic shaking at 800 rpm in a sonication bath. After 5 min of shaking the solution was kept stirring at 750 rpm in an open vial for 24 h to remove the cyclohexane by evaporation.

6.5 Encapsulation efficiency of enzymes

In order to determine the encapsulation efficiency of enzymes in the SiNCs, the capsules have to be separated from non-encapsulated enzymes in the dispersion. This separation was performed by centrifugation of 1 mL of aqueous nanocapsule dispersion at 2000*g* for 40 min at 10 °C. After this run, the precipitate was collected while the supernatant was transferred into a fresh tube for the next centrifugation step. This procedure was repeated for a total of three centrifugation runs. By using a bicinchoninic acid (BCA) protein assay the enzyme contents in the final supernatant and in the three pellets were calculated. Empty SiNCs were used as a reference sample. For the BCA assay, the BCA working reagent was prepared by mixing 25 parts of Micro BCA Reagent MA and 24 parts Reagent MB with 1 part of Reagent MC from the Micro BCA™ protein assay kit (Thermo Scientific). Diluted bovine serum albumin (BSA) solutions and diluted glucose oxidase solutions (0.5 µg/mL to 200 µg/mL) were prepared as standards. 150 µL of each standard or sample were pipetted into a microplate well of a 96-Well Plate and 150 µL of the working reagent were added. All standards and samples were measured in triplicates. The plate was covered with aluminium foil and incubated in a thermoshaker at 37 °C for 2 h. After cooling the plate to room temperature, the absorbance was recorded at 562 nm was recorded by a TECAN M1000 plate reader.

6.6 Fluorescent labeling of SiNCs

APTES was fluorescently labelled by stirring 1.16 µL of APTES with 1.66 mg Cy5-NHS-ester in 1 g of water free chloroform for 24 h. To prepare the fluorescently labelled GOx@SiNCs 2 mg of GOx were dissolved in 350 µL of DPBS using a thermoshaker at 500 rpm and 20 °C for 15 min. For the emulsion preparation, the continuous phase consisting of 10 mL of a premade solution of PGPR (26.7 mg/mL) in cyclohexane were added to the aqueous phase under magnetic stirring at 750 rpm. The mixture was homogenized with a T18 Ultra-Turrax at 13.000 rpm for 1 min. Then the emulsion was processed with a low volume microfluidizer (LV1, microfluidics corporation) with a Y-shape interaction chamber with 75 µm channels at 8000 psi in two cycles. After the emulsification, the emulsion was divided into three samples of 3 mL each and a mixture of 35 µL TMOS, 10 µL APTES and 100 µL of Cy5-APTES in chloroform was added to each sample while stirring at 750 rpm at room temperature. While stirring for 4 h at RT the reaction mixture was protected from light. Afterwards, the formed precipitate was removed by centrifugation at 300 g for 3 min at 20 °C. The transfer of the SiNCs to aqueous medium was executed in the same way as described in section 6.4.

6.7 Cell uptake

The uptake experiments were performed about a week after transferring the fluorescently labelled silica capsules to aqueous medium. The SiNC dispersion appeared homogeneous, and no indication of precipitates was observed. The SiNCs dispersion (solid content: 5 mg/mL) was diluted with Dulbecco's Modified Eagle's Medium cell culture medium (4500 mg/L glucose) with DMEM supplemented with 1% penicillin/streptomycin and 10% fetal bovine serum (FBS) (Gibco, Waltham, Massachusetts, USA) to obtain the desired SiNC concentration of 75 µg/mL.

HCT 116, a human colorectal carcinoma cell line initiated from an adult male, were used to study the cellular uptake. The HCT116 cells were obtained from ATCC (American Type Culture Collection, Manassas, USA) and cultured in DMEM containing 1% penicillin/streptomycin and 10% fetal bovine serum (FBS).

In preparation for the flow cytometry analysis, about $1.5 \cdot 10^5$ HCT 116 cells were seeded into each well of a 24-well plate (Greiner Bioone, cellstar, 662-160) in triplicates and incubated at 37 °C, 5% CO_2 overnight. The total volume per well was 1 mL. The medium was discarded and 50 µL of the diluted SiNC dispersion were added to the cells. The cells were incubated with the SiNCs for 4, 6 and 8 h at 37 °C, before discarding the medium and washing with 1 mL of DPBS. The cells were detached by adding 250 µL of Trypsin-EDTA (0.25%). After incubation at 37 °C for 2 min, 250 µL of DMEM were added and the detached cells were transferred to a 1.5 mL Eppendorf™ tube for centrifugation at 500*g* for 5 min. The pellet was resuspended in 100 µL of zombie Aqua™ dye solution (1:500 dilution in PBS), incubated at 4 °C for 15 min and centrifuged again at 500 g for 5 min. The supernatant was discarded, and the pellet was resuspended in 1 mL of DPBS, before subjecting the cells to flow cytometry measurements.

7. References

[1] C. Xu, S. Hu, X. Chen, *Mater. Today* **2016**, *19*, 516.

[2] S. M. Jo, S. Jiang, R. Graf, F. R. Wurm, K. Landfester, *Nanoscale* **2020**, *12*, 24266.

[3] S. M. Jo, F. R. Wurm, K. Landfester, *Nano Lett.* **2020**, *20*, 526.

[4] D. Wibowo, Y. Hui, A. P. J. Middelberg, C. X. Zhao, *Adv. Colloid Interface Sci.* **2016**, *236*, 83.

[5] S. Jiang, L. Caire da Silva, T. Ivanov, M. Mottola, K. Landfester, *Angew. Chem. Int. Ed.* **2022**, *61*, e202113784.

[6] M. Vert, Y. Doi, K.-H. Hellwich, M. Hess, P. Hodge, P. Kubisa, M. Rinaudo, F. Schué, *Pure Appl. Chem.* **2012**, *84*, 377.

[7] J. Potocnik, *Off. J. Eur. Communities: Legis* **2011**, *L275*, 38

[8] N. Anton, J. P. Benoit, P. Saulnier, *J. Control. Release* **2008**, *128*, 185.

[9] R. Ghosh Chaudhuri, S. Paria, *Chem. Rev.* **2012**, *112*, 2373.

[10] V. Biju, *Chem. Soc. Rev.* **2014**, *43*, 744.

[11] M. C. Daniel, D. Astruc, *Chem. Rev.* **2004**, *104*, 293.

[12] P. V. Kamat, *J. Phys. Chem. C* **2007**, *111*, 2834.

[13] V. J. Mohanraj, Y. Chen, *Trop. J. Pharm. Res.* **2006**, *5*, 561.

[14] L. Tang, J. Cheng, *Nano Today* **2013**, *8*, 290.

[15] N. Abid, A. M. Khan, S. Shujait, K. Chaudhary, M. Ikram, M. Imran, J. Haider, M. Khan, Q. Khan, M. Maqbool, *Adv. Colloid Interface Sci.* **2022**, *300*, 102597.

[16] IUPAC, *Compendium of Chemical Terminology*, 2 ed., Blackwell Scientific Publications, Oxford, **1997**.

[17] K. Landfester, *Annu. Rev. Mater. Res.* **2006**, *36*, 231.

[18] D. Crespy, K. Landfester, *Beilstein J. Org. Chem.* **2010**, *6*, 1132.

[19] M. Antonietti, *Prog. Polym. Sci.* **2002**, *27*, 689.

[20] K. Landfester, *Adv. Mater.* **2001**, *13*, 765.

[21] W. C. Griffin, *J. Soc. Cosmet. Chem.* **1949**, *1*, 311.

[22] K. Landfester, *Macromol. Rapid Commun.* **2001**, *22*, 896.

[23] K. Landfester, N. Bechthold, F. Tiarks, M. Antonietti, *Macromolecules* **1999**, *32*, 5222.

[24] K. Landfester, *Angew. Chem. Int. Ed.* **2009**, *48*, 4488.

[25] J. Hu, M. Chen, X. Fang, L. Wu, *Chem. Soc. Rev.* **2011**, *40*, 5472.

[26] Y. Zhang, B. Y. Hsu, C. Ren, X. Li, J. Wang, *Chem. Soc. Rev.* **2015**, *44*, 315.

[27] X. W. Lou, L. A. Archer, Z. Yang, *Adv. Mater.* **2008**, *20*, 3987.

[28] I. Capek, *Adv. Colloid Interface Sci.* **2010**, *156*, 35.

[29] A. Q. Zhang, H. J. Li, D. J. Qian, M. Chen, *Nanotechnology* **2014**, *25*, 135608.

[30] W. Weng, J. Lin, Y. Du, X. Ge, X. Zhou, J. Bao, *J. Mater. Chem. A* **2018**, *6*, 10168.

[31] Y. Chen, C. Chu, Y. Zhou, Y. Ru, H. Chen, F. Chen, Q. He, Y. Zhang, L. Zhang, J. Shi, *Small* **2011**, *7*, 2935.

[32] J. V. Alemán, A. V. Chadwick, J. He, M. Hess, K. Horie, R. G. Jones, P. Kratochvíl, I. Meisel, I. Mita, G. Moad, S. Penczek, R. F. T. Stepto, *Pure Appl. Chem.* **2007**, *79*, 1801.

[33] B. L. Cushing, V. L. Kolesnichenko, C. J. O'Connor, *Chem. Rev.* **2004**, *104*, 3893.

[34] A. E. Danks, S. R. Hall, Z. Schnepp, *Mater. Horiz.* **2016**, *3*, 91.

[35] C. J. Brinker, *J. Non-Cryst. Solids* **1988**, *100*, 31.

[36] K. C. Chen, T. Tsuchiya, J. D. Mackenzie, *Journal of Non-Crystalline Solids* **1986**, *81*, 227.

[37] W. Stöber, A. Fink, E. Bohn, *J. Colloid Interface Sci.* **1968**, *26*, 62.

[38] M. C. Goncalves, *Molecules* **2018**, *23*.

[39] Z. Cao, L. Dong, L. Li, Y. Shang, D. Qi, Q. Lv, G. Shan, U. Ziener, K. Landfester, *Langmuir* **2012**, *28*, 7023.

[40] S. M. Jo, H. S. Kim, M. Won, C. Champanhac, J. S. Kim, F. R. Wurm, K. Landfester, *Adv. Funct. Mater.* **2022**, 2200791.

[41] P. Schwille, J. Spatz, K. Landfester, E. Bodenschatz, S. Herminghaus, V. Sourjik, T. J. Erb, P. Bastiaens, R. Lipowsky, A. Hyman, P. Dabrock, J. C. Baret, T. Vidakovic-Koch, P. Bieling, R. Dimova, H. Mutschler, T. Robinson, T. D. Tang, S. Wegner, K. Sundmacher, *Angew. Chem. Int. Ed.* **2018**, *57*, 13382.

[42] B. C. Buddingh, J. C. M. van Hest, *Acc. Chem. Res.* **2017**, *50*, 769.

[43] J. Shi, Y. Wu, S. Zhang, Y. Tian, D. Yang, Z. Jiang, *Chem. Soc. Rev.* **2018**, *47*, 4295.

[44] S. Tsitkov, H. Hess, *ACS Catal.* **2019**, *9*, 2432.

[45] A. Küchler, M. Yoshimoto, S. Luginbuhl, F. Mavelli, P. Walde, *Nat. Nanotechnol.* **2016**, *11*, 409.

[46] S. M. Jo, F. R. Wurm, K. Landfester, *ACS Appl. Mater. Interfaces* **2018**, *10*, 34230.

[47] S. Jiang, D. Prozeller, J. Pereira, J. Simon, S. Han, S. Wirsching, M. Fichter, M. Mottola, I. Lieberwirth, S. Morsbach, V. Mailander, S. Gehring, D. Crespy, K. Landfester, *Nanoscale* **2020**, *12*, 2626.

[48] M. Li, S. Jiang, J. Simon, D. Passlick, M. L. Frey, M. Wagner, V. Mailander, D. Crespy, K. Landfester, *Nano Lett.* **2021**, *21*, 1591.

[49] S. Libertino, V. Aiello, A. Scandurra, M. Renis, F. Sinatra, *Sensors* **2008**, *8*, 5637.

[50] C. C. Chen, J. S. Do, Y. Gu, *Sensors* **2009**, *9*, 4635.

[51] P. K. Smith, R. I. Krohn, G. T. Hermanson, A. K. Mallia, F. H. Gartner, M. D. Provenzano, E. K. Fujimoto, N. M. Goeke, B. J. Olson, D. C. Klenk, *Anal. Biochem.* **1985**, *150*, 76.

[52] R. I. Krohn, *Curr. Protoc. Cell Biol.* **2011**, *Appendix 3*, 3H.

[53] M. Zhou, Z. Diwu, N. Panchuk-Voloshina, R. P. Haugland, *Anal. Biochem.* **1997**, *253*, 162.

[54] H. Schlaad, H. Kukula, J. Rudloff, I. Below, *Macromolecules* **2001**, *34*, 4302.

8. Abbreviations

APTES	(3-Aminopropyl)triethoxysilane
APTMS	(3-Aminopropyl)trimethoxysilane
BCA	Bicinchoninic acid
BSA	Bovine serum albumin
DLS	Dynamic light scattering
DMEM	Dulbecco's Modified Eagle's Medium
DPBS	Dulbecco´s sodium phosphate buffer
FBS	Fetal bovine serum
GOx	Glucose oxidase
GOx@SiNCs	Silica nanocapsules with glucose oxidase encapsulated inside their cavity
HLB	Hydrophilic-lipophilic balance
HRP	Horseradish peroxidase
HRP@SiNCs	Silica nanocapsules with horseradish peroxidase encapsulated inside their cavity
hph-SiNCs	Silica nanocapsules that were synthesized using a miniemulsion processed by high-pressure homogenization
PDI	Polydispersity index
(PE/B-*b*-PEO)	Poly(ethylene-co-butylene)-block-poly(ethylene oxide)
PGPR	Polyglycerol polyricinoleate
MADLS	Multi-Angle Dynamic Light Scattering
MFI	Median fluorescence intensity
SC	solid content
SiNC	Silica nanocapsule
son-SiNCs	Silica nanocapsules that were synthesized using a miniemulsion processed by high-pressure homogenization
TMOS	Tetramethyl orthosilicate
TEM	Transmission electron microscopy
TEOS	Tetraethyl orthosilicate
TGA	Thermogravimetric analysis

9. Appendix

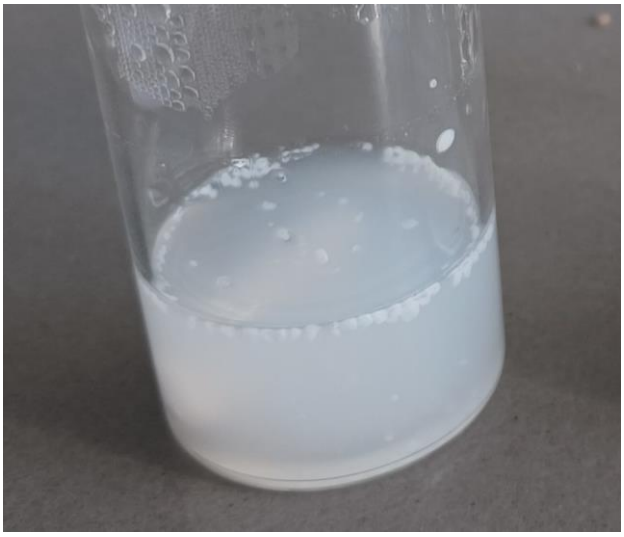

Figure 36: Photograph of the aggregates formed after redispersing the SiNCs prepared using sonication as the emulsification technique.

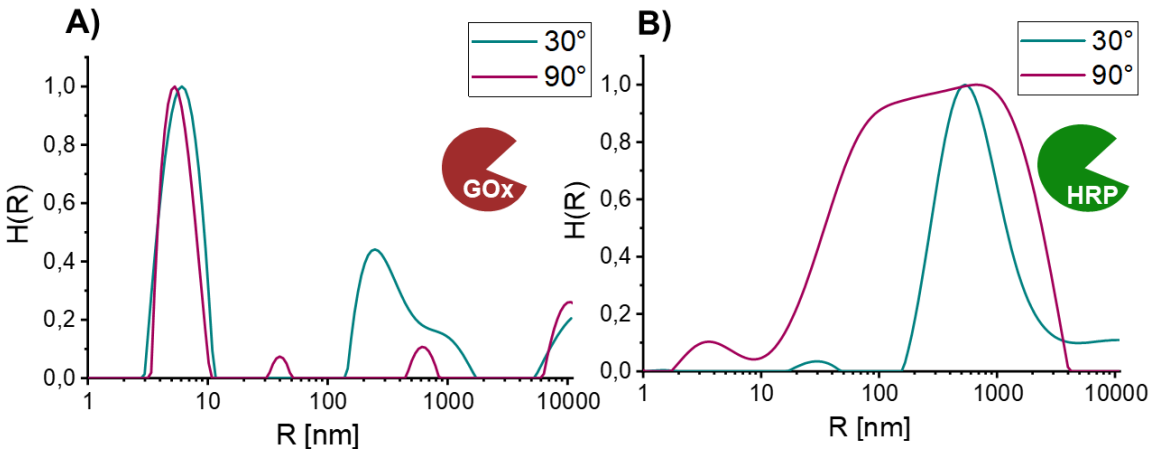

Figure 37: Distribution function H(R) of the radius R (intensity weighted) for A) 4 mg/mL glucose oxidase and B) 8 mg/mL HRP.

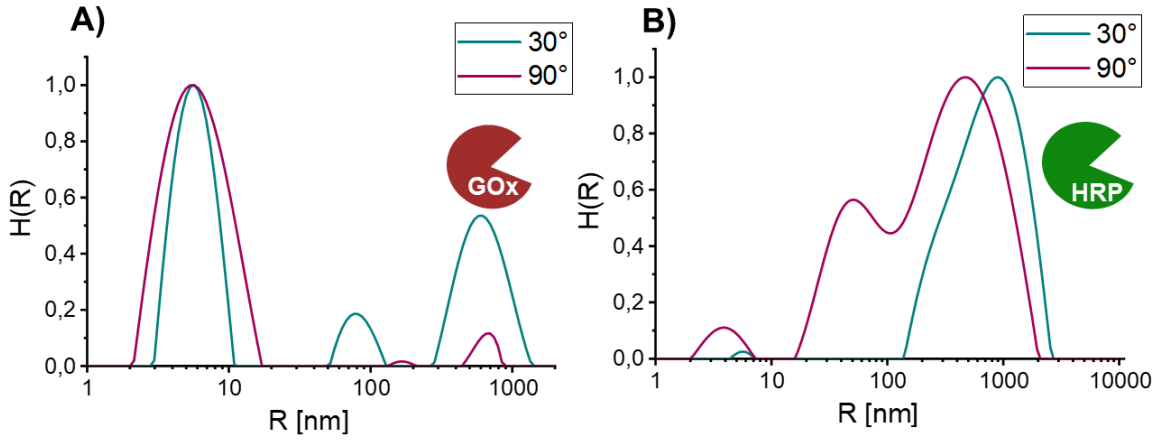

Figure 38: Distribution function H(R) of the radius R (intensity weighted) for A) 8 mg/mL glucose oxidase and B) 16 mg/mL HRP.

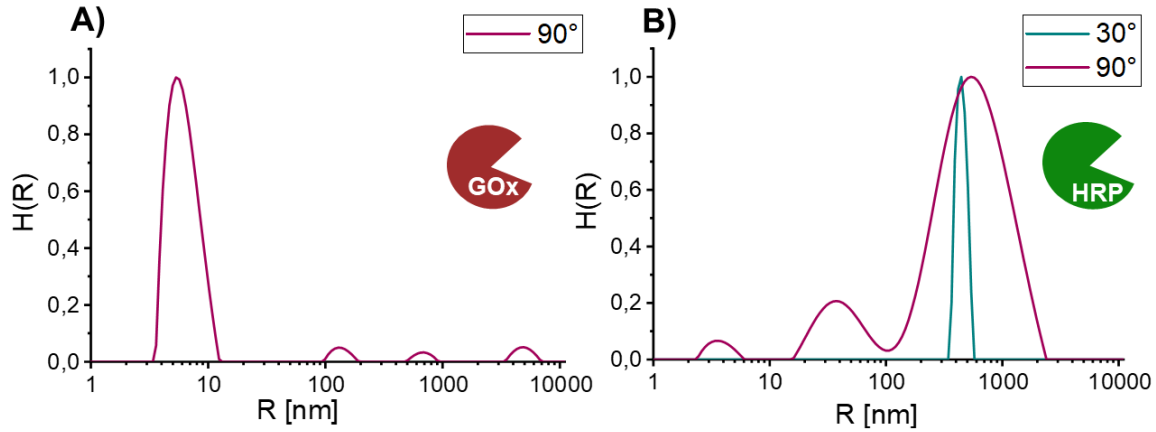

Figure 39: Distribution function H(R) of the radius R (intensity weighted) for A) 16 mg/mL glucose oxidase and B) 32 mg/mL HRP.

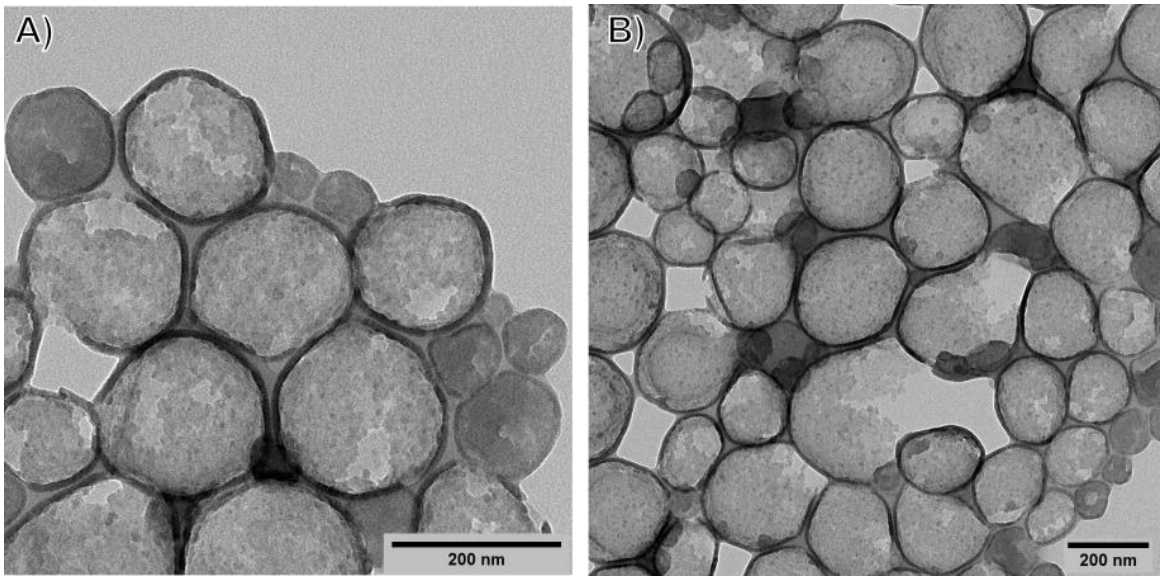

Figure 40: TEM micrographs of GOx@SiNCs with A) 10 mg/mL and B) 1 mg/mL as the GOx concentration in the dispersed phase measured in cyclohexane.

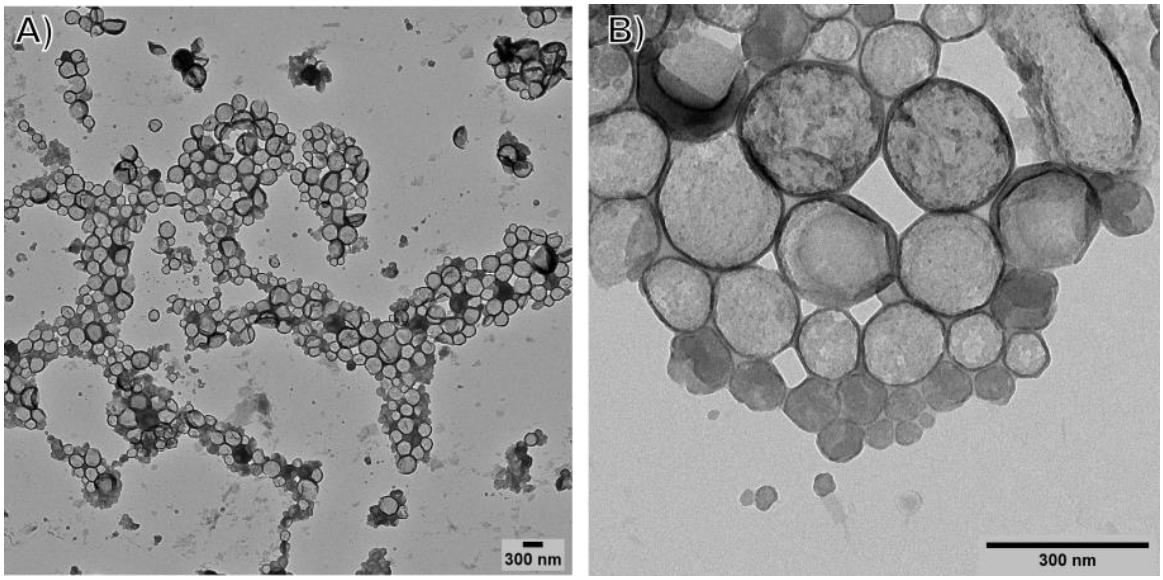

Figure 41: TEM micrographs of HRP@SiNCs with A) 10 mg/mL and B) 1 mg/mL as the HRP concentration in the dispersed phase measured in cyclohexane.

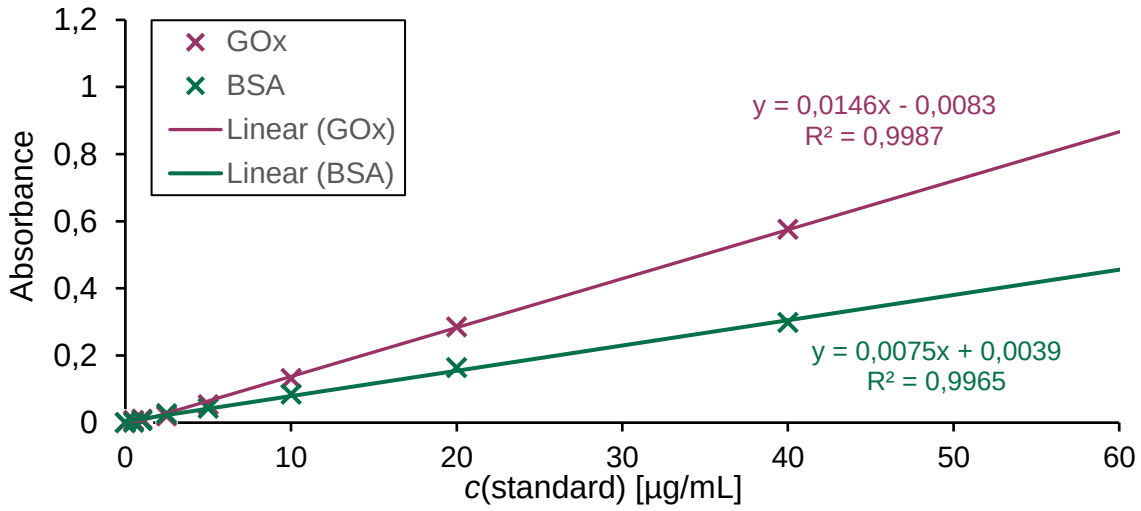

Figure 42: Calibration curves for protein quantification by BCA using either bovine serum albumin (BSA, pink) or glucose oxidase (GOx, green) for calibration.